

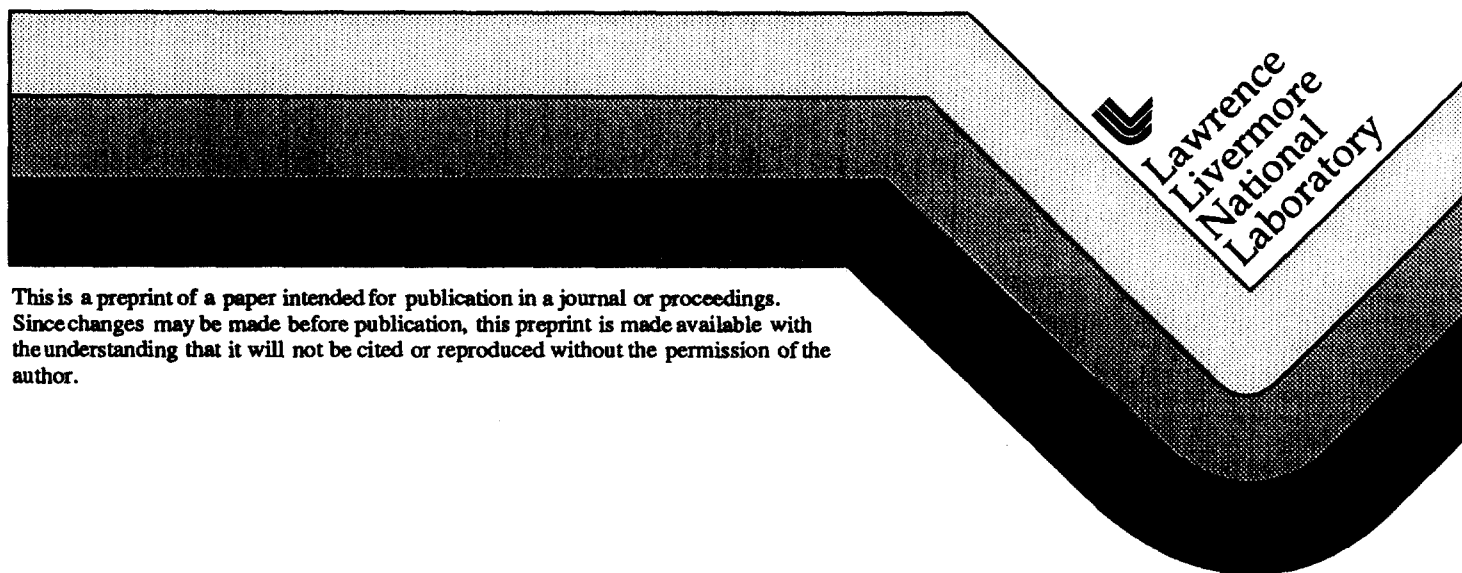
UCRL-JC-126789  
PREPRINT

# A Comprehensive Modeling Study of n-Heptane Oxidation

H.J. Curran  
P. Gaffuri  
W.J. Pitz  
C.K. Westbrook

This paper was prepared for submittal to  
*Combustion and Flame*

March 1997



#### DISCLAIMER

This document was prepared as an account of work sponsored by an agency of the United States Government. Neither the United States Government nor the University of California nor any of their employees, makes any warranty, express or implied, or assumes any legal liability or responsibility for the accuracy, completeness, or usefulness of any information, apparatus, product, or process disclosed, or represents that its use would not infringe privately owned rights. Reference herein to any specific commercial product, process, or service by trade name, trademark, manufacturer, or otherwise, does not necessarily constitute or imply its endorsement, recommendation, or favoring by the United States Government or the University of California. The views and opinions of authors expressed herein do not necessarily state or reflect those of the United States Government or the University of California, and shall not be used for advertising or product endorsement purposes.

# **A Comprehensive Modeling Study of n-Heptane Oxidation.**

H. J. Curran, P. Gaffuri, W. J. Pitz and C. K. Westbrook  
*Lawrence Livermore National Laboratory, Livermore, CA 94550*

Type: Full Length Article

Corresponding Author:

Dr. Henry J. Curran

L-407,

Lawrence Livermore National Laboratory,

Livermore,

CA, 94550

Phone: (510)-422-5790

Fax: (510)-422-6594

e-mail: [curran6@llnl.gov](mailto:curran6@llnl.gov)

# A Comprehensive Modeling Study of n-Heptane Oxidation.

H. J. Curran, P. Gaffuri, W. J. Pitz and C. K. Westbrook

*Lawrence Livermore National Laboratory, Livermore, CA 94550*

## Abstract

A detailed chemical kinetic mechanism has been developed and used to study the oxidation of n-heptane in flow reactors, shock tubes and rapid compression machines. Over the series of experiments numerically investigated, the initial pressure ranged from 1 to 42 atm, the temperature from 550 to 1700 K, the equivalence ratio from 0.3 to 1.5, and nitrogen-argon dilution from 70 to 99 percent. The combination of ignition delay time and species composition data provide for a stringent test of the chemical kinetic mechanism. The reactions are classed into various types and the reaction rates constants are given together with an explanation of how the rate constants were obtained. Experimental results from the literature of ignition behind reflected shock waves and in a rapid compression machine were used to develop and validate the reaction mechanism at both low and high temperatures. Additionally, species composition data from a continuously stirred tank reactor (CSTR) and a high pressure turbulent flow reactor were used to help complement and refine the low temperature portions of the reaction mechanism. A sensitivity analysis was performed for each of the combustion environments. This analysis showed that the low temperature chemistry is very sensitive to the formation of stable olefin species from QOOH radicals and to the chain branching steps involving ketohydroperoxide molecules.

## Introduction

There is continued interest in developing a better understanding of the oxidation of large hydrocarbon fuels over a wide range of operating conditions. This interest is motivated by the need to improve the efficiency and performance of currently operating combustors and reduce the production of pollutant species emissions generated in the combustion process. This study particularly focuses on the effect of elevated pressures on the oxidation of n-heptane. Many important practical combustion systems such as spark ignition, diesel and gas turbine engines operate at pressures well above one atmosphere. N-heptane is a primary reference fuel (PRF) for octane rating in internal combustion engines, and so a better understanding of its oxidation kinetics is useful in studies of engine knock and autoignition. Recent experimental studies of n-heptane oxidation have focused on shock tubes [1]-[5], jet stirred reactors [6, 7, 8], rapid compression machines [9]-[12], engines [13]-[19], plug flow reactors [20]-[22], and jet-stirred flow reactors [23, 24]. All of these systems exhibit phenomena including self ignition, cool flame, and negative temperature coefficient (NTC) behaviour. Furthermore, variation in pressure from 5 to 40 bar changes the temperature range over which the NTC region occurs.

Recent modeling studies of the premixed systems such as stirred reactors and shock tubes cited above [2]-[6] have helped in the development of detailed chemical kinetic mechanisms which describe n-heptane oxidation. These publications have been complemented by the work of Chevalier et al. [25, 26], Muller et al. [27], Foelsche et al. [28], and Lindstedt and Maurice [29]. In addition, Bui-Pham and Sheshadri [30] carried out a numerical study of an n-heptane diffusion flame. More recently, Ranzi et al. [31] have used a semi-detailed chemical kinetic model to simulate n-heptane pyrolysis and oxidation. In addition, this semi-detailed model was used to simulate the oxidation of primary reference fuel (n-heptane and 2,2,4-trimethyl-pentane) mixtures [22]. Côme et al. [32] have used a computer package to generate chemical kinetic mechanisms for n-heptane and iso-octane.

In this study we include all of the reactions known to be pertinent to both high and low temperature kinetics. We show how the detailed kinetic model reproduces the measured results in each type of experiment, including the features of the NTC region. We discuss the specific classes of elementary reactions and reaction pathways relevant to the oxidation process, how we arrived at the rate constants for each class of reaction, and indicate which reactions are the most important in consuming the fuel at both low and high temperature. In addition, a sensitivity analysis was carried out on each set of experimental results by changing the rate constants for different classes of reaction in the kinetic mechanism. The results of this analysis indicate the relative importance of each class of reaction and also the variation in contribution of these classes of reactions to the changing conditions of the experiments.

## Model Formulation

The present detailed reaction mechanism was constructed based on the hierarchical nature of hydrocarbon-oxygen systems. The mechanism was built in a stepwise fashion starting with small hydrocarbons and progressing to larger ones. Much of this work is documented previously [33]-[37], but has required extensive refinements. A semi-detailed kinetic scheme developed by Ranzi et al. [31, 38] in which both the low and the high temperature reaction submechanisms are reduced to a lumped kinetic model involving a limited number of intermediate steps was employed. This lumped reaction model was found to be extremely valuable in identifying portions of the detailed mechanism which were especially sensitive and which required modification and improvement.

To cover the complete range of temperature and pressure typical of n-heptane oxidation it was important to include both the low and the high temperature mechanisms. At higher temperatures, unimolecular fuel and alkyl radical species decomposition and isomerization reactions are especially important, while at low temperatures H atom abstraction from the fuel molecule and addition of alkyl radicals to molecular oxygen, followed by reactions of the alkylperoxy radicals dominate the oxidation mechanism.

The low temperature submechanism which was developed previously [34]-[37], has undergone several major changes which were necessary to explain the combustion of n-heptane in the temperature range 550–900 K. A  $\beta$ -decomposition reaction path for hydroperoxy-alkyl radicals, leading to the formation of smaller olefins and aldehydes, was included. This step has helped explain the selectivity for lower alkenes [7, 8, 12], and also increases the number of chain propagation pathways which compete with the chain branching channel in the NTC region.

Furthermore, ketohydroperoxide species have been identified during the oxidation of n-heptane in a motored CFR engine [14]. Consequently, we have added a pathway leading to the formation of ketohydroperoxide compounds from the isomerization reactions of  $\dot{O}_2QOOH$  radicals. These ketohydroperoxide species subsequently decompose producing one other hydroxyl radical (chain branching step) in addition to other oxygenated compounds. The inclusion of this step has had a large influence on the reproduction of the observed NTC behaviour and two-stage ignition of the fuel. The lumped reaction model was particularly valuable in identifying this reaction pathway as being necessary in the modeling of alkane fuels.

Finally, the THERM program [39] of Ritter and Bozzelli, which uses group additivity rules developed by Benson [40], was used to evaluate thermochemical quantities for all chemical species for which there was no available data. In addition to improving the specific heats and enthalpies of formation for many  $C_7$  compounds, it was found that reverse rate constants of many reactions in the low temperature regime were quite important, and improved thermodynamic parameters for these species provided better reverse reaction rate constants. H/C/O groups and bond dissociation groups were updated based on recent work by Bozzelli and coworkers [41].

### Classes of Reactions

We have developed our chemical kinetic model in a systematic way. The oxidation of any fuel takes place through a series of steps. For example, at both low and high temperature n-heptane undergoes H atom abstraction, leading to the formation of four possible, structurally distinct alkyl radicals. At high temperatures these radicals decompose *via*  $\beta$ -scission to yield a smaller olefin and another radical species. However, at low temperatures these four alkyl radicals undergo addition to  $O_2$  leading to the formation of four heptylperoxy radicals. Therefore, we can categorize each step in the oxidation process as a class of reaction, including all the possible reactions taking place. These classes of reactions are listed below, and indicate the complexity of the model. The complete reaction mechanism for n-heptane oxidation included 2450 elementary reactions among 550 chemical species. The entire mechanism is not represented here due to its length, but we discuss below its contents, and a complete copy can be obtained from the authors in either printed or electronic form.

We have found many reaction types to be important and particular attention and care has been taken in developing rate constant expressions for these reaction classes. However, not all reactions have been found to be important, and we have at times been expedient in our treatment of certain reaction types. For example, in our treatment of H atom abstraction from  $C_7$  alkene species, we assume only one alkenyl radical is produced, which is taken as an 'average' over the species possible for n-heptane. Furthermore, we have also simplified alkenyl consumption to consist only of unimolecular decomposition to products we have selected as being reasonable for the fuel. Thus, n-heptane, a straight-chained fuel, is assumed to lead to alkenyl decomposition products with allyl radicals and olefins. This treatment is very approximate, and further attention may be warranted, but this has proven adequate for our current applications. The major classes of elementary reactions considered in the present mechanism include the following:

1. Unimolecular fuel decomposition
2. H atom abstraction from the fuel
3. Alkyl radical decomposition

4. Alkyl radical + O<sub>2</sub> to produce olefin + HÖ<sub>2</sub> directly
5. Alkyl radical isomerization
6. Olefin abstraction reactions by ÖH, H, Ö, and ÖCH<sub>3</sub>
7. Olefin addition reactions
8. Alkenyl radical decomposition
9. Olefin decomposition
10. Addition of alkyl radicals to O<sub>2</sub>
11.  $\dot{R} + R'\dot{O}_2 = R\dot{O} + R'\dot{O}$
12. Alkyl peroxy radical isomerization ( $R\dot{O}_2 \rightleftharpoons \dot{Q}OOH$ )
13.  $R\dot{O}_2 + H\dot{O}_2 = RO_2H + O_2$
14.  $R\dot{O}_2 + H_2O_2 = RO_2H + H\dot{O}_2$
15.  $R\dot{O}_2 + CH_3\dot{O}_2 = R\dot{O} + CH_3\dot{O} + O_2$
16.  $R\dot{O}_2 + R'\dot{O}_2 = R\dot{O} + R'\dot{O} + O_2$
17.  $RO_2H = R\dot{O} + \dot{O}H$
18. RÖ decomposition
19.  $\dot{Q}OOH = QO + \dot{O}H$  (epoxide formation *via* cyclisation of diradical)
20.  $\dot{Q}OOH = \text{olefin} + H\dot{O}_2$  (radical site  $\beta$  to OOH group)
21.  $\dot{Q}OOH = \text{olefin} + \text{carbonyl} + \dot{O}H$  (radical site  $\gamma$  to OOH group)
22. Addition of  $\dot{Q}OOH$  to O<sub>2</sub>
23. Isomerization of  $\dot{O}_2QOOH$  and formation of ketohydroperoxide and ÖH
24. Decomposition of ketohydroperoxide to form oxygenated radical species and ÖH
25. Epoxide reactions with ÖH and HÖ<sub>2</sub>

The naming conventions used above are  $\dot{R}$  and  $R'$  denoting alkyl radicals or structures and  $Q$  denoting C<sub>n</sub>H<sub>2n</sub> species or structures. For each of these classes of reactions we use the same reaction rate constant for analogous occurrences in different molecules. Thus, we assume that the abstraction of a tertiary H atom by reaction with ÖH radicals has exactly the same rate in 2-methyl butane, 2-methyl pentane, 3-methyl pentane and in iso-octane. Correspondingly, the total rate of tertiary H atom abstraction by ÖH in 2,3-dimethyl butane and in 2,4-dimethyl pentane is twice that in 2-methyl pentane, since the two former fuels have two such H atoms at tertiary sites.

## Summary of High Temperature Mechanism

Reactions in classes 1–9 are sufficient to simulate many high temperature applications of n-heptane oxidation. We have made a number of *ad hoc* assumptions and approximations that may not be suitable for some problems involving alkene and alkyne fuels and further analysis is needed to refine details for these fuels. However, under the conditions of this study, n-heptane oxidation is relatively insensitive to these assumptions.

### Reaction type 1: Unimolecular fuel decomposition

These reactions produce two alkyl radicals or one alkyl radical and one H atom. Because the paths producing H atoms have very high activation energies, they are only important in the reverse direction, where they serve as sinks of H atoms. Type 1 reactions serve as initiation steps and as fuel consumption reactions but only at relatively high temperatures, such as those found in shock tubes.

We calculate the rate constant expressions for unimolecular decomposition of n-heptane fuel from the reverse reaction, the recombination of two radical species to form the stable parent fuel, and from microscopic reversibility. For products of alkyl + H atom we assume a rate constant for recombination of  $1 \times 10^{14} \text{ cm}^3 \text{ mol}^{-1} \text{ s}^{-1}$ , based on the recommendation of Allara and Shaw [42]. There is very little information available on the rate of this reaction for  $\text{C}_2$  alkyl radicals and larger. For decompositions where the smallest product is  $\dot{\text{C}}\text{H}_3$  we assume the reverse recombination rate to be  $1.0 \times 10^{13} \text{ cm}^3 \text{ mol}^{-1} \text{ s}^{-1}$ , similar to that recommended by Baulch et al. [43] for  $\dot{\text{C}}\text{H}_3 + \dot{\text{C}}\text{H}_3 = \text{C}_2\text{H}_6$ . When the smallest product is an alkyl radical such as ethyl or larger we assume the recombination rate constant to be  $8.0 \times 10^{12} \text{ cm}^3 \text{ mol}^{-1} \text{ s}^{-1}$ .

### Reaction type 2: H atom abstraction

At both low and high temperatures H atom abstraction takes place at both primary and secondary sites of n-heptane, which leads to the formation of four distinct heptyl radicals. There are no tertiary sites on the n-heptane molecule, but we have included these rate constant expressions so that we can provide a complete set, and these will be used in modeling iso-octane oxidation.

We assume that the rate constant for abstraction at any particular site ( $1^\circ$ ,  $2^\circ$  or  $3^\circ$ ) to be equal to that at the same type of site in other molecules. For example, we chose the rate constant for H atom abstraction by  $\dot{\text{O}}\text{H}$  radicals at both primary and secondary sites to be identical to those recommended by Droege and Tully [44] for propane fuel. The rate constant for tertiary H atom abstraction by  $\dot{\text{O}}\text{H}$  radicals was taken from a similar study by the same authors [45] with isobutane fuel. We summarize these rate constant expressions in Table 1, and calculate the reverse rate constants from thermochemistry.

### Reaction type 3: Alkyl radical decomposition

Alkyl radical decomposition is important only at relatively high temperatures ( $T > 850 \text{ K}$ ) under the conditions of this study, as the addition of alkyl radicals to molecular oxygen, even though a bimolecular reaction, is faster than  $\beta$ -scission due to the relatively high activation energy barriers for alkyl radical decomposition (there is no energy barrier for the addition to  $\text{O}_2$ ). Generally, we have chosen products based on the principle that  $\beta$ -scission will be the dominant decomposition path for alkyl radicals. In many cases there are two or more pathways possible for an alkyl radical, with different products, and all such paths have been included in the present mechanism.

Previously, we treated this type of reaction in the forward direction estimating the rate constant for each  $\beta$ -scission by analogies with similar reactions. However, because alkyl radical  $\beta$ -scission is endothermic we now calculate the rate constant in the reverse, exothermic direction i.e. the addition of an alkyl radical (or H atom) across the double bond of an alkene. In this way we avoid the additional complexity of the enthalpy of reaction, allowing the forward,  $\beta$ -scission rate constant to be calculated from thermochemistry.

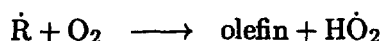
Rate constants for the addition of radicals across a double bond are reasonably well known and are very similar depending on (1) the site of addition (terminal or internal C atom) and (2) the type of radical



adding on. We use rate constants for these addition reactions based on the recommendations of Allara and Shaw [42]. Typically, the rate of addition of a  $\dot{\text{H}}$  atom across a double bond has a pre-exponential  $A$ -factor of  $1 \times 10^{13} \text{ cm}^3 \text{ mol}^{-1} \text{ s}^{-1}$  with an activation energy of 1200 cal/mol if the  $\dot{\text{H}}$  atom adds to the terminal C atom of the alkene, and 2900 cal/mol if the  $\dot{\text{H}}$  atom adds to an internal C atom. The rate constant for the addition of an *alkyl* radical has a lower  $A$ -factor and higher activation energy than for the addition of a H atom. For the addition of an alkyl radical, the  $A$ -factor is approximately  $8.5 \times 10^{10} \text{ cm}^3 \text{ mol}^{-1} \text{ s}^{-1}$  with an activation energy of approximately 7800 cal/mol if addition occurs at the terminal C atom and 10600 cal/mol higher if addition occurs at an internal C atom. We assume these reactions are in their high pressure limit for the conditions considered in this study.

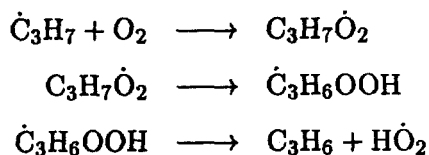
#### Reaction type 4: $\text{Alkyl} + \text{O}_2 = \text{olefin} + \text{H}\dot{\text{O}}_2$

The reaction of alkyl radicals with  $\text{O}_2$  proceeds through many reaction channels. Most of these channels can be represented by the addition of alkyl radicals to  $\text{O}_2$ , reaction type 10, followed by alkyl peroxy radical isomerization to hydroperoxy-alkyl radical, reaction type 12, and subsequent decomposition or further addition of the the hydroperoxy-alkyl radical to  $\text{O}_2$ , reaction types 19 to 22. Reaction type 4 proceeds through a vibrationally excited  $\text{R}\dot{\text{O}}_2^*$  radical and refers to the fraction of these chemically excited  $\text{R}\dot{\text{O}}_2$  adducts which lead to the formation of an olefin and  $\text{H}\dot{\text{O}}_2$  radical directly.



The reaction mechanism leading to the formation of conjugate olefin from alkyl plus  $\text{O}_2$  is a topic of considerable current research. Schaefer and coworkers [55] have proposed that  $\text{C}_2\text{H}_5 + \text{O}_2$  reacts through a cyclic transition state and then proceeds directly to ethylene plus  $\text{H}\dot{\text{O}}_2$  through a concerted elimination. This proposed reaction sequence does not proceed through the  $\dot{\text{Q}}\text{OOH}$  radical. This is in agreement with the earlier proposals of Walker and co-workers [56, 57], in which they suggested that a pathway involving a cyclic quasi-stable structure must exist, without the prior formation of  $\text{C}_2\text{H}_5\text{O}_2$ , which can either decompose back into  $\text{C}_2\text{H}_5 + \text{O}_2$  or unimolecularly decompose into  $\text{C}_2\text{H}_4 + \text{H}\dot{\text{O}}_2$ . However, Wagner et al. [58] argue that were this cyclic intermediate to exist,  $\text{H}\dot{\text{O}}_2$  would also react with  $\text{C}_2\text{H}_4$  forming  $\text{C}_2\text{H}_5 + \text{O}_2$  to a significant extent instead of exclusively forming  $\dot{\text{C}}\text{H}_2\text{CH}_2\text{O}_2\text{H}$ , followed by the subsequent formation of ethylene oxide  $\text{C}_2\text{H}_4\text{O} + \dot{\text{O}}\text{H}$ . No evidence of such behaviour was observed by Walker and coworkers. Thus, questions concerning the kinetic behaviour of the  $\text{C}_2\text{H}_5 + \text{O}_2 \rightarrow \text{C}_2\text{H}_4 + \text{H}\dot{\text{O}}_2$  reaction sequence remain. However, all proposed alkyl radical plus  $\text{O}_2$  reactions do lead to the formation of the conjugate olefin and  $\text{H}\dot{\text{O}}_2$ .

Koert et al. [59] showed that only about 10 percent of the propene produced from propane oxidation occurs through Reaction type 4 over the NTC region at 10 to 15 atm. The remaining 90 percent of the propene is formed through the addition of the alkyl radical to  $\text{O}_2$ , isomerization of propyl-peroxy radical to hydroperoxy-propyl radicals, and subsequent decomposition to form propene plus  $\text{H}\dot{\text{O}}_2$ .



It is expected that the contribution of reaction type 4 will decrease significantly with increasing number of carbon atoms in the alkyl radical. There are  $3N-6$  modes of vibration possible for a non-linear molecule, where  $N$  is the number of atoms in the molecule. The addition of an alkyl radical to  $\text{O}_2$  results in  $\approx 34.0 \text{ kcal mol}^{-1}$  of energy in the C-O bond formed. As the number of carbon atoms in a molecule increases this excess energy is more easily delocalized throughout the molecule via all possible vibrations, this lowers the probability of the C-O bond breaking and thus the  $\text{R}\dot{\text{O}}_2$  adducts will have a longer lifetime.

Therefore, the  $\text{RO}_2$  radicals can undergo collisional stabilization, especially under the high pressure (13.5–40 bar) conditions of this study. For this reason, we have not included reaction type 4 in the present study for alkyl radical containing more than four carbon atoms. We have obtained good agreement between experimental and computational results for both  $\text{C}_5$  and  $\text{C}_6$  species using this assumption [60, 61].

#### Reaction type 5: Alkyl radical isomerization

Alkyl radicals can transfer H atoms from one site to the vacant site at rates that depend on the type of C-H bond (primary, secondary or tertiary) broken, and the ring strain energy barrier involved. This process has been well known for many years and was summarized by Benson [40]. The rate constants for isomerization are described in terms of the number of atoms in the transition state ring structure (including the H atom) and the type of site at which the transferred H atom was initially located. Thus, we estimate the activation energy,  $\mathcal{E}_a$ , using the expression,

$$\mathcal{E}_a = \Delta H_{\text{rxn}} + \text{ring strain} + E_{\text{abst}} \quad (1)$$

where  $\Delta H_{\text{rxn}}$  is taken to be the enthalpy of reaction and is only included if the reaction is endothermic. The activation energy for abstraction is determined, following the analysis of Bozzelli and Pitz [62], from an Evans-Polanyi plot ( $E_{\text{abst}}$  vs  $\Delta H_{\text{rxn}}$ ) of similar H atom abstraction reactions,  $\text{RH} + \dot{\text{R}}' = \dot{\text{R}} + \text{R}'\text{H}$  leading to the following expression:

$$E_{\text{abst}} = 12.7 + (\Delta H_{\text{rxn}} \times 0.37)$$

The  $\mathcal{A}$ -factors were obtained using RADICALC [63], a computer code that implements transition state theory. RADICALC calculates the change in entropy of the radical to the transition state due to loss or gain of internal rotors, of specific vibrations, and of optical isomers. A more in-depth description of the use of RADICALC has been published by Bozzelli and Pitz [62]. We consider only H atom transfers, excluding  $\dot{\text{C}}\text{H}_3$  or larger radical transfers. The rate constants used heptyl radical isomerizations are summarized in Table 2.

#### Reaction type 6: Olefin abstraction reactions

Although smaller olefin species are always important in virtually all combustion environments, larger olefin species are generally much less important. At high temperatures, alkyl radicals decompose rapidly to smaller olefins, while at lower temperatures the  $\text{RO}_2$  reaction paths, which produce small quantities of large olefins, tend to dominate. As a result, we have chosen not to include a great deal of detail in the reactions of the larger olefins.

We have assumed that for olefins larger than  $\text{C}_4$ , each alkene can have H atoms abstracted by  $\dot{\text{H}}$ ,  $\dot{\text{O}}$ ,  $\dot{\text{O}}\text{H}$  and  $\dot{\text{C}}\text{H}_3$ . However, because (1) site-specific abstraction rate constants are more difficult to estimate for olefins than for paraffins, (2) the number and complexity of the product species become difficult to follow, (3) the fate of those products are not very well understood and (4) the sensitivity of the computed results to variations in these steps is very small, we decided to assume a single rate expression for reactions of all of these large olefins with each of the radical species. An approximate rate value is assumed for each abstracting radical, intended to provide a rate constant averaged over primary, secondary, tertiary, and allylic C-H sites. As olefins get larger in carbon number, the double bond affects only a small portion of the molecule, the rest of which remains paraffinic in character. Thus, for large olefins, we expect the rate constants for H atom abstraction to look more like those for alkanes than small olefins. Furthermore, for each fuel, only one alkenyl radical is assumed to be produced, a sort of ‘average’ over the species possible for that fuel.

This type of treatment is expedient in the current study, and modifications would be needed in cases of specific interest. For example, if the study considered a large olefin as the primary fuel, this approach would be inappropriate and refinements would be necessary. The rate constant expressions estimated in this mechanism are reported in Table 3.

### Reaction type 7: Olefin addition reactions

Similar to the discussion of type 6 reactions, we have tried to account for the possible addition reactions of small radicals with large olefin species. We have already considered the addition reactions of olefins with  $\dot{\text{H}}$  and  $\dot{\text{CH}}_3$ , as part of type 3,  $\beta$ -scission reactions above.

$\dot{\text{O}}\text{H}$  and  $\dot{\text{O}}$  addition occurs at the double bond, which occupies only a small portion of a large olefin. Thus the  $A$ -factors below have been reduced to reflect the steric factor associated with the probability of an  $\dot{\text{O}}\text{H}$  or  $\dot{\text{O}}$  radical reacting with the olefinic rather than the paraffinic part of the molecule.

For addition of  $\dot{\text{O}}\text{H}$  and  $\dot{\text{O}}$  radicals, we have used simplified structural arguments to suggest which radical species would result from additions at the double bond, and we have tried to guess which bonds would be broken in the adduct when it then decomposes. This is a very rough and qualitative way of proceeding, and we have no illusions that the results are either unique or accurate. However, this procedure is sufficient over the range of conditions applicable to this study, but we do not advocate its 'correctness' or its adequacy in other classes of model applications. The specific reaction rate constants we have assumed are reported in Table 4.

### Reaction type 8: Alkenyl radical decomposition

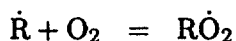
Since the process of alkenyl radical production has been greatly simplified, we have also chosen to simplify alkenyl consumption to consist only of unimolecular decomposition to products we selected as being 'reasonable' for the fuel. Thus, *n*-heptane, a straight-chain fuel, is assumed to lead to alkenyl decomposition products of allyl radicals and olefins. The rate constants of these alkenyl decompositions are all assumed to be  $2.5 \times 10^{13} \exp(-45000/RT) \text{ s}^{-1}$ . This treatment is very approximate, and further attention is warranted, but this has proven adequate for our current applications.

### Reaction type 9: Olefin decomposition

We have found that in computed models, the large olefin species decompose at appreciable rates, and these reactions must be included. We have used a rate constant of  $2.5 \times 10^{16} \exp(-71000/RT) \text{ s}^{-1}$  recommended by Edelson and Allara [49] for 1-hexene decomposition for all of these reactions, and we have tried to select product distributions which would be expected on structural and thermochemical grounds. This is another area in which further work would improve the mechanism.

## Low Temperature Mechanism

At temperatures lower than approximately 900 K, the high activation energies associated with the  $\beta$ -scission of alkyl radicals make these processes rather slow. Under such conditions, the most important reactions for alkyl radicals  $\text{R}$ , consist of addition to molecular oxygen:



followed by internal H atom abstraction, a second addition to  $\text{O}_2$ , H atom abstraction and subsequent decomposition to yield two reactive hydroxyl radicals and a carbonyl radical. In many ways, the first addition of an alkyl radical to  $\text{O}_2$  is the most important reaction for low temperature oxidation, even though it does not immediately determine the overall rate of chain branching. Pollard [65] carried out an extensive kinetic analysis of hydrocarbon oxidation under low temperature conditions, and identified the most important features of the low temperature submechanism. Many recent modeling studies have incorporated these features in their mechanisms. Most of these models assume that the chemical details of fuel autoignition are so complex that significant simplifications are essential in order to be able to simulate the oxidation process. Some of the most prominent of these simplified model treatments of hydrocarbon ignition are the "Shell Model" [66] and related developments by Hu and Keck [67] and Cox and Cole [68]. A recent survey and critical analysis of these simplified approaches by Griffiths [69] has summarised the strengths and limitations of these models. However, recent studies in detailed kinetic

modeling of hydrocarbon oxidation [35, 60, 61] have made it possible to address a wide variety of issues related to ignition, most of them leading to improved descriptions of ignition in internal combustion engines and engine knock.

#### Reaction type 10: $\dot{R} + O_2$ addition

Following Benson [70], additions involving alkyl radicals larger than  $C_4$  to  $O_2$  were assumed to have the same bimolecular rate constant of  $2 \times 10^{12} \text{ cm}^3 \text{ mol}^{-1} \text{ s}^{-1}$ . The reverse decomposition rate constants are calculated from microscopic reversibility. We assume that the  $RO_2$  radical is rapidly stabilized to its ground state as there are 66 (3N-6) modes of vibration in the  $C_7H_{15}O_2$  radical and so the energy released during C-O bond formation is easily dissipated throughout the molecule. In addition, collisional stabilization is fast under the high pressure (13.5–40 bar) conditions of this study. The activation energy for the addition reaction is taken to be zero but is quite large  $\approx 30 \text{ kcal/mol}$  in the reverse dissociation direction. Therefore, the equilibrium constant for this reaction is very strongly temperature dependent. At very low temperatures this reaction proceeds rapidly to produce the alkylperoxy species very efficiently; at high temperatures  $RO_2$  dissociates rapidly and the concentration of  $RO_2$  is very small. This point is clearly related to the concept of "ceiling" temperature [70], defined as that temperature at which  $[R][O_2]/[RO_2] = 1$ . Pressure also influences the  $\dot{R} + O_2 = RO_2$  equilibrium, so for engine knock or other elevated pressure problems these submechanisms continue to be important at temperatures higher than at atmospheric pressure.

#### Reaction type 11: $\dot{R} + R'O_2 = RO + R'\dot{O}$

Reactions of alkyl radicals with alkylperoxy radicals are assumed to occur at:

$$\begin{array}{ll} 1.9 \times 10^{12} \exp(+1200/RT) \text{ cm}^3 \text{ mol}^{-1} \text{ s}^{-1} & \text{forward} \\ 1.0 \times 10^{10} \text{ cm}^3 \text{ mol}^{-1} \text{ s}^{-1} & \text{reverse} \end{array}$$

The forward rate is based on the value of Kaiser et al. [71] for the reaction  $\dot{C}H_3 + CH_3\dot{O}_2 = CH_3\dot{O} + CH_3\dot{O}$ . They recommend an  $A$ -factor of  $3.8 \times 10^{12}$  with an activation energy of  $-1200 \text{ cal/mol}$  equal to that given above. We have reduced this  $A$ -factor by two as the  $C_7 \dot{R}$  and  $R'\dot{O}_2$  radicals are larger than the  $\dot{C}H_3$  and  $CH_3\dot{O}_2$  radicals, and therefore we expect a reduced rate of reaction. The reverse rate constant is estimated.

#### Reaction type 12: $RO_2$ isomerization

Our treatment of these reactions has been adopted from Benson [70], Pollard [65], and Bozzelli and Pitz [62]. In addition to the four  $RO_2$  species formed by the addition of heptyl radicals to  $O_2$ , there are eighteen possible QOOH isomers produced by internal H atom abstraction of these  $RO_2$  radicals. Figure 1 depicts 2-heptylperoxy radical undergoing one of five possible isomerization reactions, considering intermediate ring structures as large as 8 members, via a six membered transition state (T.S.) ring structure. This T.S. structure undergoes rapid stabilization, transfers a secondary H atom, and forms 2-hydroperoxy-4-heptyl radical.

The way in which we calculate the activation energy for  $RO_2$  isomerization is identical to that described for alkyl radical isomerization. Rate constants depend on (1) ring strain energy barriers, (2) the type and location of the abstracted H atom ( $1^\circ$ ,  $2^\circ$ , or  $3^\circ$ ), and (3) the degeneracy or number of H atoms at that site. However, it was found that, in order to correctly predict relative concentrations of heterocyclic products reported in the literature [7, 12], it was necessary to lower the ring-strain energy for the change in going from a six membered, (1,5p), to a seven membered, (1,6p), T.S. ring by  $2.8 \text{ kcal mol}^{-1}$  and not  $4.8 \text{ kcal mol}^{-1}$  as recommended by Baldwin et al. [72]. We arrive at a lower activation energy for the 7-membered ring as do Baldwin et al., which is in some contrast to alkyl radical isomerizations, where 6-membered rings are preferred. Nonetheless, in keeping with the alkyl radical isomerization analogy we do increase the ring strain energy in going from a (1,6) to a (1,7) T.S. ring choosing a value of  $2.8 \text{ kcal mol}^{-1}$ . The

approximate ring strain energies used in this study are reported in Table 5. Thus for example, we calculated the activation energy for the five membered, primary (1,4p) T.S. to be 29.2 kcal mol<sup>-1</sup> using equation 1, which is similar to 30.0 kcal mol<sup>-1</sup> which is the value reported by Wagner et al. [73] for the (1,4p) T.S. internal H atom abstraction in the ethylperoxy radical leading to the formation of ethylhydroperoxide. We chose a value of 29.7 kcal mol<sup>-1</sup> a number which lies between both of the above values. The pre-exponential *A*-factor is assumed to decrease with increasing ring size due to the loss of internal rotors. This consideration is the main contributor to the decrease in entropy of the transition state [62]. The *A*-factor depends linearly on the number of equivalent H atoms being abstracted. The *A*-factor for the (1,4p) T.S. ring was chosen to be  $8.9 \times 10^{12} \text{ s}^{-1}$ , a value approximately the same as that recommended by Baldwin et al. [72]. This value is reduced for the (1,5p) T.S. ring by a multiple of 12, assuming a change in entropy,  $\Delta S \approx 5.0 \text{ cal mol}^{-1} \text{ K}^{-1}$ , and in increments of 12 for all singular changes in T.S. ring size thereafter.

These reactions are reversible, and again we calculate the reverse isomerization using thermochemistry. Although Pollard and Benson discuss rate constant expressions in a general way, detailed study of this class of reaction has only recently received considerable attention, and there is still some question about the correct energy barriers to these processes. It is possible that some of the disagreements or lack of unanimity is due to analyses at different pressures and temperatures that might affect stabilization of the excited  $\dot{\text{R}}\text{O}_2^*$  radical. However, as already noted, for the applications in this study, we expect stabilization of  $\dot{\text{R}}\text{O}_2^*$  to be very rapid and so our treatment should be appropriate. We summarize our recommended rates of  $\dot{\text{R}}\text{O}_2$  isomerization in Table 6.

#### Reaction type 13: $\dot{\text{R}}\text{O}_2 + \text{H}\dot{\text{O}}_2 = \text{RO}_2\text{H} + \text{O}_2$

It should be noted that this class of reaction is bimolecular, the rate of reaction depending on  $k[\dot{\text{R}}\text{O}_2][\text{H}\dot{\text{O}}_2]$ . The concentrations of both radical species, although high relative to other species in the oxidation process, will typically be of the order of  $10^{-6} \text{ moles cm}^{-3}$  or less. This infers that the unimolecular isomerization  $\dot{\text{R}}\text{O}_2 \rightleftharpoons \dot{\text{Q}}\text{OOH}$  (type 12) will inevitably be much faster than this bimolecular reaction. Nonetheless, the balance between  $\text{H}\dot{\text{O}}_2$  and other radicals is often of great importance in these problems and so this reaction type is included in our mechanism. This reaction, when followed by the decomposition of  $\text{RO}_2\text{H}$ , converts  $\text{H}\dot{\text{O}}_2$  to  $\dot{\text{O}}\text{H}$ , which can accelerate the overall rate of reaction. However, the  $\text{RO}_2\text{H}$  species is quite stable, and at sufficiently low temperature, this reaction terminates chain branching and reduces the overall rate of reaction. There is not much information available on this reaction type except for the case when  $\dot{\text{R}}$  is  $\dot{\text{C}}\text{H}_3$ . For this class of reaction we have assumed a rate expression:

$$\begin{array}{ll} 1.0 \times 10^{11} \text{ cm}^3 \text{ mol}^{-1} \text{ s}^{-1} & \text{forward} \\ 3.0 \times 10^{11} \exp(-39000 \text{ cal/RT}) \text{ cm}^3 \text{ mol}^{-1} \text{ s}^{-1} & \text{reverse} \end{array}$$

Our rate choice is somewhat lower than the recommendation of Wallington et al. [74] who give a rate constant expression of  $3.1 \times 10^{11} \exp(+1272 \text{ cal/RT}) \text{ cm}^3 \text{ mol}^{-1} \text{ s}^{-1}$  in the temperature range 228–573 K, where  $\dot{\text{R}}$  is  $\dot{\text{C}}\text{H}_3$ . The reaction showed no pressure dependence over the pressure range of 25–760 torr. This rate constant yields  $7.74 \times 10^{11} \text{ cm}^3 \text{ mol}^{-1} \text{ s}^{-1}$  at 700 K. However, we expect the rate constant to decrease with increasing size of the  $\dot{\text{R}}$  radical and therefore our recommended rate constant is lower. Because of lack of data, we have neglected the small negative activation energy in our choice.

#### Reaction type 14: $\dot{\text{R}}\text{O}_2 + \text{H}_2\text{O}_2 = \text{RO}_2\text{H} + \text{H}\dot{\text{O}}_2$

This is an interesting reaction sequence that converts one stable species and a peroxy species into another stable species and another peroxy species. The subtlety in the reaction and its influence on the overall reaction sequence is due to the differences in the temperatures at which the  $\text{RO}_2\text{H}$  and  $\text{H}_2\text{O}_2$  species decompose.  $\text{RO}_2\text{H}$  decomposes at a lower characteristic temperature than  $\text{H}_2\text{O}_2$ . Conversion of  $\text{H}_2\text{O}_2$  to  $\text{RO}_2\text{H}$  leads to an enhanced overall reactivity at lower temperatures. We have used rate constant expressions that are the same in both forward and reverse directions,

$$2.4 \times 10^{12} \exp(-10000 \text{ cal/RT}) \text{ cm}^3 \text{ mol}^{-1} \text{ s}^{-1}$$

There is little information available for this reaction rate constant except for the case where  $\dot{R}$  is  $\dot{C}H_3$ . Our choice of rate constant is based on Tsang's recommendation [75] for  $CH_3\dot{O}_2 + H_2O_2 = CH_3O_2H + \dot{H}O_2$  of  $k = 2.41 \times 10^{12} \exp(-9940 \text{ cal/RT}) \text{ cm}^3 \text{ mol}^{-1} \text{ s}^{-1}$  from 300–2500 K with an uncertainty of a factor of 5. For this isoergic reaction, the reverse rate is the same as the forward rate by analogy.

**Reaction type 15:  $R\dot{O}_2 + CH_3\dot{O}_2 = R\dot{O} + CH_3\dot{O} + O_2$**

This sequence converts peroxy radicals to others radicals which decompose more readily. The reaction rate constants are not particularly well known, but we have estimated the forward rate constant of the reaction to be  $1.0 \times 10^{11} \text{ cm}^3 \text{ mol}^{-1} \text{ s}^{-1}$  and the trimolecular reverse reaction rate is set to zero, since the three body reaction is not expected to proceed. There is little information available for  $\dot{R}$  other than  $\dot{C}H_3$ . Our rate constant choice agrees well with the recommended rate constant of  $CH_3\dot{O}_2 + CH_3\dot{O}_2 = CH_3\dot{O} + CH_3\dot{O} + O_2$  from the recent review of Wallington et. al. [74]. They give a total rate of  $CH_3\dot{O}_2 + CH_3\dot{O}_2$  leading to products, in addition to a branching ratio in the temperature range 250–600 K. No pressure effect in the total rate was observed from 10–760 torr. Using this information, Wallington et al. recommend a rate constant expression of  $6.9 \times 10^{10} \exp(+22 \text{ cal/RT}) \text{ cm}^3 \text{ mol}^{-1} \text{ s}^{-1}$  for the  $CH_3\dot{O} + CH_3\dot{O} + O_2$  product channel which yields  $8 \times 10^{10} \text{ cm}^3 \text{ mol}^{-1} \text{ s}^{-1}$  at 700 K. We have neglected this small, negative activation energy in our extrapolation to other analogous reactions.

**Reaction type 16:  $R\dot{O}_2 + R'\dot{O}_2 = R\dot{O} + R'\dot{O} + O_2$**

This is another reaction which interconverts  $R\dot{O}$  and  $R\dot{O}_2$  radical species. The rate is estimated to be  $1.0 \times 10^{11} \text{ cm}^3 \text{ mol}^{-1} \text{ s}^{-1}$  with a zero reverse reaction rate. We were unable to find any information for cases where  $\dot{R}$  and  $\dot{R}'$  are different alkyl radicals. When  $\dot{R} = \dot{R}'$ , Wallington et al. gives  $6.81 \times 10^{10} \exp(-664 \text{ cal/RT}) \text{ cm}^3 \text{ mol}^{-1} \text{ s}^{-1}$  for  $\dot{R} = \dot{C}_2H_5$  and 260–380 K. This rate constant gives  $4.2 \times 10^{10}$  at 700 K. Wallington's review also recommends  $1.39 \times 10^{12} \exp(-5090 \text{ cal/RT}) \text{ cm}^3 \text{ mol}^{-1} \text{ s}^{-1}$  for  $\dot{R} = i\dot{C}_3H_7$  and 300–373 K which yields  $3.6 \times 10^{10} \text{ cm}^3 \text{ mol}^{-1} \text{ s}^{-1}$  at 700 K.

**Reaction type 17:  $R\dot{O}_2H = R\dot{O} + \dot{O}H$**

It had been thought in the past that this reaction step was important as it produces two very reactive radical species. However, as already explained for type 13 reactions above,  $R\dot{O}_2$  radical preferentially undergoes the unimolecular isomerization to  $\dot{Q}OOH$ . Therefore, very small concentrations of stable  $RO_2H$  species are formed in the low temperature oxidation process. For completeness, these reactions have been maintained in our mechanism. Using THERM, we have generated more reliable thermodynamic data for both reactant and product species of this reaction class, and have assigned a rate constant of  $k = 1.0 \times 10^{13} \text{ cm}^3 \text{ mol}^{-1} \text{ s}^{-1}$  for the reverse radical-radical addition reaction, calculating the forward decomposition rate constant from microscopic reversability.

**Reaction type 18:  $R\dot{O}$  decomposition**

The alkoxy radicals that are produced in the oxidation process are quite unstable and tend to decompose quite readily. Large alkoxy radicals can decompose into smaller oxygenated species, primarily aldehydes or ketones, together with an alkyl species. We have used an analogy with  $\beta$ -scission to identify the product distribution and estimate a rate constant expression of  $2.0 \times 10^{13} \exp(-15000 \text{ cal/RT}) \text{ s}^{-1}$  for these reactions. With this activation energy, this reaction will be rapid only in the higher ranges of temperature in our applications, where the product alkyl radical should also be expected to decompose. As a result we have combined these two steps into one overall global reaction, with a zero reverse rate. Since aldehydes are generally quite reactive, and the alkyl products also lead to radical species production, the process of  $R\dot{O}$  decomposition can contribute to reaction acceleration.

**Reaction type 19:  $\dot{\text{QOOH}} = \text{QO} + \dot{\text{OH}}$** 

This reaction sequence involves the breaking of the O-O bond, coupled with the formation of a cyclic compound including the remaining O atom. We have followed the recommendations of Pollard [65], in which the activation energy barrier depends on the size of the cyclic species ring which is formed. However, we have altered the rate constants of these reactions from those published previously [34, 35, 36]. Taking into account loss in entropy as described earlier, we again reduce the pre-exponential factor by a multiple of 12 as one extra rotor is tied up in going from a 3 to 4 and progressively larger ring heterocycles. The activation energies have also been altered in order to model correctly cyclic ether distributions measured experimentally. The six-membered ring tetrahydropyran species are assumed to have the lowest ring-strain energy, while the oxirane species are assumed to have the greatest strain energy. The rate parameters we use for these reactions are reported in Table 7.

**Reaction type 20:  $\dot{\text{QOOH}} = \text{olefin} + \text{H}\dot{\text{O}}_2$** 

$\dot{\text{QOOH}}$  species that have a radical site beta to the hydroperoxy group can decompose to yield a conjugate olefin and  $\text{H}\dot{\text{O}}_2$  radical. The rate constant for this reaction was considered in the reverse direction i.e. the addition of an  $\text{H}\dot{\text{O}}_2$  radical at an olefinic site, in the same way as alkyl radical decomposition (type 3 above). The energy barrier for the addition reaction is better known than is the decomposition of the alkylhydroperoxide to products. Thus, following analogy rules for addition of a radical to a double bond, a rate constant of  $8.5 \times 10^{10} \exp(-7800 \text{ cal/RT}) \text{ cm}^3 \text{ mol}^{-1} \text{ s}^{-1}$  was chosen for olefin +  $\text{H}\dot{\text{O}}_2$  similar to the value recommended by Tsang [76] for the reaction:  $\dot{\text{C}}\text{H}_3 + \text{C}_3\text{H}_6 = \text{isoC}_4\text{H}_9$ . The forward rate constant is calculated from thermochemistry. This reaction has proven to be quite sensitive, and is responsible for a large part of the NTC behaviour in n-heptane oxidation kinetics.

**Reaction type 21:  $\dot{\text{QOOH}} = \text{olefin} + \text{carbonyl} + \dot{\text{OH}}$** 

$\dot{\text{QOOH}}$  species, produced by an  $\text{R}\dot{\text{O}}_2$  isomerization with an intermediate ring structure of 6 atoms can undergo  $\beta$ -scission. Scission products were chosen considering the weakest interatomic bonds in the molecule. We have chosen a rate constant of  $5.0 \times 10^{13} \exp(-25500/\text{RT}) \text{ s}^{-1}$  which is similar to that recommended by Pollard [65], for each of these  $\beta$ -scission reactions. Since the reverse reaction is trimolecular, its rate is assumed to be negligible.

**Reaction type 22: Addition of  $\dot{\text{QOOH}}$  to  $\text{O}_2$** 

Finally,  $\dot{\text{QOOH}}$  can react with molecular oxygen to form peroxyalkylhydroperoxide,  $\dot{\text{O}}_2\text{QOOH}$ , species. A rate constant of  $2 \times 10^{12} \text{ cm}^3 \text{ mol}^{-1} \text{ s}^{-1}$  was chosen, consistent with the value chosen for alkyl plus  $\text{O}_2$ , type 10. The reverse dissociation rate was then calculated from thermochemistry using THERM.

**Reaction type 23:  $\dot{\text{O}}_2\text{QOOH}$  isomerization to ketohydroperoxide +  $\dot{\text{OH}}$** 

One of the main additions to the current mechanism is the treatment of the decomposition of the  $\dot{\text{O}}_2\text{QOOH}$  species formed. Based on the experimental observations reported by Sahetchian et al. [15], in which heptyl-ketohydroperoxides are observed, we assume that the  $\dot{\text{O}}_2\text{QOOH}$  isomerizes releasing  $\dot{\text{OH}}$  and forming different ketohydroperoxide species depending on the  $\dot{\text{O}}_2\text{QOOH}$  involved. For example, Figure 2 depicts 2-hydroperoxy-5-heptylperoxy radical undergoing isomerization through a seven membered transition state ring structure, forming 5-hydroperoxy-2-heptanone. The rate constant for this and other isomerizations via an internal H atom transfer are analogous to those for  $\text{R}\dot{\text{O}}_2 \rightleftharpoons \dot{\text{QOOH}}$  isomerization, and are reported in Table 8. However, the activation energy has been reduced by 3 kcal mol<sup>-1</sup> as the hydrogen atom being abstracted is bound to a carbon atom which is bound to a hydroperoxy group and should be more easily removed. In addition, the A-factor has also been reduced by a factor of 0.5 considering steric hinderance due to the OOH group. These reactions are very important in the modeling of two-step ignition phenomena observed in shock tubes [5], CFR engines [13]-[15] and rapid compression machines [9, 12].

#### Reaction type 24: Ketohydroperoxide decomposition

One reactive hydroxyl radical is formed during the production of ketohydroperoxide species. The subsequent decomposition of ketohydroperoxide molecules leads to the formation of two radicals, a carbonyl radical and another  $\dot{\text{O}}\text{H}$  radical, providing chain branching as it produces two radical species from one stable reactant. It is especially important that formation and decomposition of ketohydroperoxide molecules produce two  $\dot{\text{O}}\text{H}$  radicals in the present mechanism. Griffiths [69] reported that multiplication of reaction chains is curtailed by displacement from branching to non-branching reaction modes, that the  $\dot{\text{O}}\text{H}$  radical is considerably more reactive than the  $\text{H}\dot{\text{O}}_2$  radical and that considerable exothermicity is associated with  $\dot{\text{O}}\text{H}$  radical propagation, while  $\text{H}\dot{\text{O}}_2$  propagation is virtually thermoneutral.

A single rate constant of  $1.0 \times 10^{16} \exp(-43000 \text{ cal/RT}) \text{ s}^{-1}$  was chosen for the decomposition of each ketohydroperoxide molecule even though each ketohydroperoxide species has slightly different thermodynamic properties. Our rate constant expression is similar to  $4.0 \times 10^{15} \exp(-42924 \text{ cal/RT}) \text{ s}^{-1}$  recommended by Baluch et al. [43] for the decomposition of the ethylhydroperoxide molecule,  $\text{C}_2\text{H}_5\text{O}_2\text{H} = \text{C}_2\text{H}_5\dot{\text{O}} + \dot{\text{O}}\text{H}$ . This set of reactions is especially important at low temperatures as the high activation energy ensures an induction period in which ketohydroperoxide concentration builds up and when they subsequently decompose, the decomposition products help accelerate the overall rate of fuel oxidation, raising the temperature and allow the remaining ketohydroperoxide species to decompose more easily.

#### Reaction type 25: Epoxide reactions with $\dot{\text{O}}\text{H}$ and $\text{H}\dot{\text{O}}_2$

The detailed reaction mechanisms of most epoxide species are not well established. Lifshitz et al. [77, 78] investigated the pyrolysis of ethylene oxide, and oxidation of ethylene oxide, propylene oxide and two epoxybutanes behind reflected shock waves. However, very little chemical kinetic data is reported other than Arrhenius-type correlation equations pertaining to the global oxidation of fuel/oxygen mixtures diluted with both argon and nitrogen. Baldwin et al. [79] reported rate constant expressions for H atom abstraction from ethylene oxide by  $\dot{\text{H}}$ ,  $\dot{\text{O}}\text{H}$  and  $\dot{\text{C}}\text{H}_3$ , including the subsequent decomposition of the oxiranyl radical to  $\dot{\text{C}}\text{H}_3 + \dot{\text{C}}\text{O}$ . More recently, Dagaut et al. [80] have published a paper including speciation data and kinetic parameters of reactions associated with ethylene oxide oxidation. However, this study was carried out mainly at high temperatures where ethylene oxide isomerizes to acetaldehyde.

Cyclic ethers are produced under low temperature conditions during hydrocarbon oxidation and, in the present study are relatively large  $\text{C}_7$  species with an O atom embedded in the molecule. Therefore, it is reasonable to assume that the reaction proceeds by means of H atom abstraction followed by unimolecular decomposition. We have made some assumptions relating to site of H atom abstraction and the nature of the product species formed in these reactions. We assume that the ease of H atom abstraction will be in the following order  $3^\circ > 2^\circ > 1^\circ$ . In addition, a H atom bound to a carbon atom which is bound to the oxygen atom in the ring structure will be more easily abstracted. Furthermore, we have assumed that only H atom abstraction by  $\dot{\text{O}}\text{H}$  radical and  $\text{H}\dot{\text{O}}_2$  radicals will be of any great importance, because these radicals are in highest concentrations at low temperature. We adopt two sets of product distributions for abstraction reactions by  $\dot{\text{O}}\text{H}$  radicals, and two more for abstractions by  $\text{H}\dot{\text{O}}_2$ . We have tried to include rate constants for these various H atom abstraction reactions by drawing analogies with similar reactions published in the literature. Abstraction of primary and tertiary H atoms from a cyclic ether by  $\dot{\text{O}}\text{H}$  radical was taken to be equal to the values for  $1^\circ$  and  $3^\circ$  H atom abstraction from isobutane recommended by Tully et al. [45]. Secondary H atom abstraction was taken to be equal to that recommended by Droege and Tully [44] for  $2^\circ$  H atom abstraction from propane. Abstraction of a H atom bonded to a  $1^\circ$  carbon atom which in turn is bonded to an oxygen atom was taken to be four times faster than abstraction from a typical  $2^\circ$  H atom. Abstraction of a H atom bonded to a  $2^\circ$  carbon atom which in turn is bonded to an oxygen atom was taken to be approximately three times faster than the rate recommended by Walker [81] for  $3^\circ$  H atom abstraction from isobutane. These rate constant expressions are summarized in Table 9. Primary and tertiary H atom abstraction from a cyclic ether by  $\text{H}\dot{\text{O}}_2$  was taken to be equal to the values for  $1^\circ$  and  $3^\circ$



H atom abstraction from isobutane recommended by Tsang [82]. Secondary H atom abstraction was taken to be equal to that recommended by Tsang [83] for 2° H atom abstraction from propane. Abstraction of a 2° H atom bonded to a carbon atom which is bonded to an oxygen atom was taken to be four times faster than a typical 2° H atom and abstraction of a 3° H atom by  $\dot{\text{H}}\text{O}_2$  at a similar site was taken to be approximately three times faster than a typical 3° H atom.

### Reaction Mechanism

The overall flux diagram for n-heptane oxidation can be shown schematically in a particularly simple way as seen in Figure 3. At high temperatures, the overall reaction pathway proceeds *via*  $\beta$ -scission of the alkyl radicals  $\dot{\text{R}}$  proceeding rapidly to a smaller olefin and other species, with chain branching due primarily to the reaction  $\dot{\text{H}} + \text{O}_2 = \dot{\text{O}} + \dot{\text{O}}\text{H}$ . At low temperatures, chain branching is mainly due to the reaction pathway leading through the ketohydroperoxide species. As the temperature increases, the chain propagation reactions of  $\dot{\text{Q}}\text{OOH}$  species increase, because the energy barrier to their formation is more easily overcome, leading to the formation of epoxide species, conjugate olefins, and  $\beta$ -decomposition products, at the expense of the reaction pathways through the ketohydroperoxide species. The increasing importance of these propagation channels leads to a lower reactivity of the system which is observed as the NTC region. The difference in the chain branching mechanisms at low and high temperatures leads to varying reactivity depending on the fuel to air equivalence ratio. Because the chain branching mechanism at high temperatures is due to the  $\dot{\text{H}} + \text{O}_2 = \dot{\text{O}} + \dot{\text{O}}\text{H}$  reaction, fuel lean mixtures are more reactive in this regime. However, at low temperatures, because chain branching is dependant on radical species formed directly from the parent fuel, fuel rich mixtures are oxidized more quickly.

### Mechanism Validation

An explanation of the chemical kinetic mechanism formulation has been given in the preceding section. In order to validate this mechanism it is necessary to carry out simulations of experimental measurements available in the literature. In the following section we describe how this mechanism was used to simulate experimental results obtained in a plug flow reactor [20, 22], a jet-stirred reactor [6, 7, 8], shock tubes [1]-[5] and rapid compression machines [9]-[12]. Except for the shock tube studies of Vermeer et al. [1] and Coats and Williams [2], these studies involve n-heptane oxidation over temperatures at which NTC behaviour can be clearly observed.

#### Variable Pressure Flow Reactor

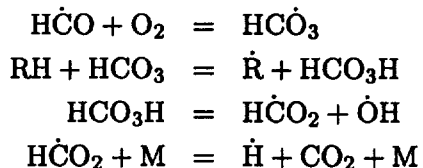
Experiments, carried out in an adiabatic flow reactor, provide a well-characterized environment that is designed to minimize mixing and diffusion effects. Details of the experimental apparatus are provided by Dryer et al. [22, 20]. N-heptane was studied under stoichiometric air to fuel ratios, the initial concentration of fuel was approximately 0.14%, with a high amount of nitrogen diluent, approximately 99%. Experiments were performed over an initial temperature range of 550–850 K, and at a constant pressure of 12.5 atm. The residence time was fixed at 1.8 s. The initial temperature of the  $\text{O}_2/\text{N}_2$  carrier gas was set at a particular value and the entire reactor system, without fuel flow, was allowed to thermally equilibrate. Fuel flow was then commenced and, after stabilization of the analytical measurement readings, data were obtained for the mole fraction of CO,  $\text{CO}_2$ ,  $\text{H}_2\text{O}$ ,  $\text{O}_2$ , and the temperature at the fixed sampling location. The axial distance from the fuel vapour injection location to the sampling location was varied for each initial flow temperature to maintain the reaction residence time constant. Fuel flow was then turned off and the initial reactor temperature incrementally changed. The entire procedure was repeated at the new initial reactor temperature.

The results indicate quite clearly the characteristic NTC behaviour of n-heptane oxidation. Figure 4 shows the  $\text{O}_2$  and CO concentrations measured at 1.8 s as a function of initial  $\text{O}_2/\text{N}_2$  temperature.  $\text{O}_2$

concentrations below 1.6% indicate consumption of  $O_2$  in the reactor. Consumption of  $O_2$  and production of CO indicate that the n-heptane (not measured in the reactor) was consumed. The consumption of n-heptane begins at about 560 K and increases until fuel consumption peaks at 600 K. The calculations show that the reactivity from 560–600 K is due to the consumption of ketohydroperoxide species leading to the formation of reactive  $\dot{O}H$  radicals. At initial temperatures less than 600 K, the  $\dot{Q}OOH$  radical preferentially adds to molecular oxygen leading to chain branching, rather than undergoing decomposition. At initial temperatures above 600 K fuel consumption gradually decreases up to a temperature of about 730 K. This decrease in reactivity, characteristic of NTC behaviour, is caused by the competitive decomposition of the  $\dot{Q}OOH$  radical to form olefin and  $H\dot{O}_2$ , cyclic ether and  $\dot{O}H$  or  $\beta$ -scission products, all of which are chain propagation paths and provide reduced overall reactivity than the chain branching ketohydroperoxide pathway. At initial temperatures greater than approximately 760 K the radical pool becomes well established and dissociation of hydrogen peroxide into two hydroxyl radicals leads to rapid consumption of the remaining fuel.

### Jet Stirred Reactor

Recently Dagaut et al. [7, 8] reported experimental results on the oxidation of n-heptane in a jet-stirred reactor at 10 and 40 atm covering the low and the high temperature regimes (550–1150 K) with equivalence ratios from 0.3 to 1.5, and 99% dilution by nitrogen. These experimental results are especially valuable since both the reactant concentrations and intermediate and final product concentrations were measured. A series of comparisons between computed and experimental results is shown in Figure 5 for stoichiometric mixtures of 0.11% n-heptane in oxygen/nitrogen at 10 atm and a residence time of 1 s. From the model results, it is clear that below 750 K, oxidation takes place through a low temperature mechanism leading to the formation of CO,  $CO_2$ ,  $CH_2O$ ,  $CH_3CHO$ ,  $C_2H_5CHO$ , and major intermediates including heptenes and cyclic ethers. All of these species concentrations are reproduced quite well by the model. The accurate prediction of these species levels relies heavily on the relative rates of alkylperoxy radical isomerization reactions, and the fate of the  $\dot{Q}OOH$  radical, ultimately leading to the formation of the different heptenes and cyclic ethers. It is interesting to note that most of the  $CO_2$  is being produced by a reaction sequence that has not been previously reported in the literature:



where RH is the fuel or a stable hydrocarbon intermediate.

As seen in Figures 5 and 6, the distinct NTC behaviour measured between 640 and 750 K is also reproduced well by the model. However, the model shows a lower overall reactivity than the experiments. In the reaction mechanism, product species distributions for the thermal decomposition reactions of the ketohydroperoxide species were postulated, since experimental evidence for these product distributions were unavailable. Additional refinements in this area of the mechanism could improve the model results at the low temperatures.

Above 750 K oxidation takes place *via* a higher temperature mechanism in which the most important branching reaction is the decomposition of hydrogen peroxide  $H_2O_2 \rightleftharpoons \dot{O}H + \dot{O}H$ . The model description of this system could not be accurately reproduced without including falloff corrections for this reaction rate constant. We have used the recent rate constant expression of Marinov and Malte [85] which gives a nine parameter, pressure dependent fit. Variations in equivalence ratio at constant pressure were found to change the overall reactivity of this system but did not change the temperature range of the NTC region, as is evident from Figure 6a. Model calculations at a higher pressure of 40 atm and a residence time of 2 s

showed an apparent reduction of the NTC region (Figure 6b), in agreement with experimental observation.

### Shock Tube

The autoignition of n-heptane can be studied conveniently at high temperatures in shock tubes and at lower temperatures in rapid compression machines. We have used the model to examine high temperature shock tube experiments of Vermeer et al. [1] and Coats and Williams [2]. Vermeer et al. studied the autoignition of n-heptane-oxygen mixtures behind reflected shock waves over the pressure range of 1-4 atm and the temperature interval of 1200-1700 K. Stoichiometric fuel-oxygen mixtures had to be diluted with 70% argon to reduce the influence of the boundary layer. Coats and Williams studied the ignition of n-heptane/O<sub>2</sub>/Ar mixtures behind both incident and reflected shock waves with equivalence ratios of 0.5 to 4.0 in the temperature range 1300-2000 K. Poor agreement between simulated and measured ignition delay times was observed for the Vermeer et al. experimental results, Figure 7a, but we attained good agreement with the measurements of Coats and Williams, Figure 7b. The experimental trend that fuel-lean mixtures autoignite more easily than fuel-rich mixtures at high temperature (1300-2000 K) is also reproduced. We are unclear as to why we have poor agreement with the results of Vermeer et al. and at the same time obtain good agreement with the results of Coats and Williams in which the fuel and oxygen is highly diluted in 98% argon. The reason for this discrepancy is currently under investigation. It may be that including fall-off for these decomposition reactions would lead to longer predicted ignition delay times and better agreement with the Vermeer experimental results.

Ciezki and Adomeit [5] also carried out reflected shock tube experiments but at somewhat lower temperatures and rather high pressures, observing NTC behaviour at temperatures between 750 and 1000 K. Computed results are compared with data in Figure 8, showing overall excellent agreement between computed and measured results. The experimental trend that fuel-rich mixtures autoignite more easily than fuel-lean mixtures from 750 to 950 K is well reproduced by the model, and is in contrast with the trend we observed both experimentally and computationally for ignition delay times at high temperatures, in which fuel-lean mixtures burned faster than fuel-rich mixtures, Figure 7b. The temperature range of 750-950 K and a pressure of 13.5-40 bar are close to the conditions observed in the unburnt gas of a spark ignition engine, where engine knock occurs. These experimental and modeling results agree with automotive engine experience that fuel-rich mixtures have a greater tendency to autoignite and lead to knock than do stoichiometric or fuel-lean mixtures. The magnitude of the NTC region is very closely reproduced by the reaction mechanism. Perhaps most importantly, the shift in the NTC region to higher temperatures as pressure is increased is also accurately reproduced. This shift is due to the influence of pressure on the equilibria of the addition reactions of molecular oxygen to the alkyl and hydroperoxy-alkyl radicals. Chevalier et al. [25, 26] obtained similar results when they used their model to simulate these same experiments.

### Rapid Compression Machine

The experiments of Ciezki and Adomeit could cover only a small part of the low temperature region because of limitations in measuring long ignition times. Similar conditions have been investigated experimentally by Minetti et al. [12] in a rapid compression machine (RCM). These experiments are characterized by ignition delay times of the order of 20-40 ms. Experiments were carried out at a compression ratio of 9.8. Stoichiometric mixtures of fuel and 'air' were used, the 'air' composing 21% oxygen and 79% diluent. The diluent used consisted of mixtures of nitrogen, argon and carbon dioxide which have much different heat capacities. In this way, the compressed gas temperature could be varied by selecting different ratios of diluents; the highest temperatures were obtained when the diluent consisted entirely of argon, and the lowest temperatures with the greatest concentration of carbon dioxide. The initial gas pressure was 162 torr at an initial temperature of 355 K. In the simulations, we used the experimentally measured pressure at the end of compression and the temperature as the initial conditions for a constant volume calculation.

The compressed gas temperatures are calculated from the initial conditions of pressure, temperature and reactant composition, the pressure at top dead centre (TDC) and the temperature dependence of the ratio of specific heats  $\gamma$ , according to the equation:

$$\int_{T_0}^{T_c} \frac{\gamma}{\gamma - 1} \frac{dT}{T} = \ln \frac{P_1}{P_0}$$

In these experiments at temperatures below about 850 K, a noticeable two-stage ignition process as shown in Figure 9a is observed. A typical example of the results is shown as the bottom curve in Figure 9a, where the temperature at the end of compression is 661 K. This mixture ignites in two distinct stages, the first occurring at about 25.2 ms after the end of compression, and the second occurring at 32.4 ms. As the ratio of argon/nitrogen/carbon dioxide is increased, the post compression temperature increases and the overall ignition delay time becomes shorter, as shown by the second curve ( $T_c = 738$  K) in Figure 9a, and both the first and second ignition stages occur earlier. As the Ar/N<sub>2</sub> ratio is further increased, the system falls within the NTC region, as indicated by the third curve at 829 K, and the total ignition delay time actually increases with increasing compressed gas temperature. At this point, the first stage ignition is hardly discernable, and the increase in total ignition delay is clearly equivalent to an increase in the second stage of ignition.

The results in Figure 9a actually represent computed results based on the kinetic model, but these results have been shown to agree well with the experimental results, Figure 9b. The model reproduces the absolute delay times for both the first and second stages of ignition. Observe that the ignition becomes essentially a single-stage ignition as the temperature exceeds 810 K, although the NTC region does not disappear until the temperature exceeds 850 K. The intricate interactions in the reaction mechanism responsible for this complex behaviour are severely tested by these experiments.

In rapid compression machine experiments, the question often arises as to whether or not there is heat loss to the combustion chamber walls and whether significant reaction takes place during the compression stroke, especially when the compression time is comparable to the induction period as is the case of the Minetti et al. experiments, in which the compression time is 60 ms.

Recent RCM experiments have been carried out by Griffiths et al. [9]-[11] in order to address the two-fold question of reaction during the compression stroke and heat loss to the chamber walls. Experiments were carried out at a compression ratio of 11:1 with a compression stroke duration of 22 ms. Stoichiometric mixtures of fuel and diluent were used, in the same way as in the Minetti experiments. The initial temperature of the gas mixture before compression was 327 K at a pressure of 250 torr. The temperature of the chamber walls were assumed to remain constant at 340 K.

The model was used to simulate the overall progress of reaction, beginning at the start of the compression stroke. As in the experiments, the initial mixture temperature was 327 K, and the diluent concentrations were selected to vary the compression temperature. In this study, two sets of simulated compression histories were computed similar to the Minetti experiments, both neglecting heat losses to the combustion chamber walls. The first consisted of a full kinetic calculation including both reactions and heat release during the compression stroke, followed by the constant volume calculation throughout the ignition period. In the second set of calculations, it was assumed that no reaction occurred during the compression stroke and a fresh charge of fuel/O<sub>2</sub>/diluent was used for the constant volume ignition delay calculations. The results of these two sets of computations are shown in Figure 10a, and are labeled reactive and unreactive. Below 780 K, the two sets of calculations show the same ignition delay time as a function of the computed mixture temperature at the end of compression, showing that essentially no fuel consumption or other reaction takes place during the compression phase. As the mixture composition is adjusted further to increase the temperature following compression, the model shows that the extent of reaction during compression begins to increase. In particular, the concentrations of ketohydroperoxide

species increase. At a temperature of about 830 K, these species start to decompose, leading to rapid chain branching and rapid heat release.

At this point, a second factor becomes important, the equilibrium of the addition reaction between alkyl radicals and molecular oxygen. This reaction represents the transition between the high and low temperature reaction regimes; at temperatures above some limiting value, the equilibrium of this reaction lies on the side of the alkyl radical and molecular oxygen, while at lower temperatures the alkylperoxy radical is formed and the low temperature regime is important. It is interesting to note that, regardless of the ratio of argon to nitrogen, for all of the mixtures in Figure 9a that show a two-stage ignition, the first stage ends when the gas temperature reaches 850–900 K. For each mixture, the first ignition is largely associated with ketohydroperoxide species decomposition at a temperature between 800 and 850 K, and the end of the first stage occurs when the temperature reaches a level where the equilibrium of the  $\dot{R} + O_2 = R\dot{O}_2$  reactions begin to shift towards dissociation at about 900 K, thereby shutting off the low temperature branching reaction paths.

An important conclusion of the present modeling study is that reaction during the compression phase leads to a dependence of ignition delay time on compression temperature as shown in the reactive curve in Figure 10a. The long flat region from 750–850 K is due to fuel consumption and heat release during the final portions of the compression stroke. However, if a modeling study assumes that no reaction occurs during compression and that the initial temperature for computation is that reached at the end of compression, the computed ignition delay times would appear to be like the unreactive curve in Figure 10a. This familiar s-shaped curve would be expected on the basis of many theoretical studies, but it bears little resemblance to actual experimental results over the temperature range from 800–1000 K.

The question as to whether or not there was any heat loss to the chamber walls was also addressed. In order to determine an overall heat transfer coefficient an unreactive mixture of n-heptane and diluent in the absence of oxygen was analysed experimentally, undergoing both the compression and constant volume portions of the experiment. The initial conditions were identical to those described for reactive experiments above, with the mixture containing n-heptane/nitrogen/argon in the ratio 1:20:32.5. The pressure profile for this experiment was recorded and is shown as the points in Figure 10b. Clearly, there is indeed some heat loss, indicated by a pressure drop, the large part of which occurs at the end of compression just as the piston comes to rest. This same mixture was simulated numerically, treating the combustion chamber as a homogeneous reactor, and varying the volume with time to simulate the compression. Spatial temperature variations in the reactor were neglected, treating heat loss as a distributed heat transfer rate, proportional to the temperature difference between the average gas temperature and the time averaged wall temperature. The coefficient of proportionality is an effective heat transfer coefficient that was determined in the following manner. We varied the heat transfer coefficient to reproduce as closely as possible the pressure history measured in the unreactive experiment of Griffiths et al., the result of which can be seen as the line in Figure 10b.

A third set of RCM simulations was then carried out using the same heat loss submodel, and also including the effects of chemical reaction during the compression stroke. The computed results are shown in Figure 10a and show better agreement with the experimental results than when either heat losses or reaction during compression are neglected. A final refinement in which spatial variations in compressed gas temperature are included in a coupled kinetics/fluid mechanics model was not carried out in this study, although Griffiths [69] has previously examined this issue, using a somewhat simplified kinetic mechanism.

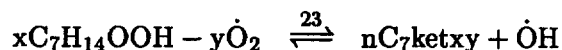
### Sensitivity Analysis

A detailed analysis was carried out to investigate the sensitivity of each class of reaction denoted earlier, to the oxidation of n-heptane. We have tried to focus our attention on low temperature kinetics as these have the greater impact on engine knock chemistry, and so we did not include sensitivity analyses of the shock tube experiments of Vermeer et al. [1] or Coats and Williams [2], where only high temperature kinetics are

important. In analysing the chemistry edits produced as output from the model, we were able to develop a flux diagram of the major oxidation pathways responsible for n-heptane oxidation, as seen in Figure 3. For this reason, our analysis has focused on the classes of the reaction mechanism which are represented in Figure 3 and we assume all others are of minor importance. Furthermore, we did not include sensitivity to other reactions such as  $\dot{\text{O}}\text{H} + \dot{\text{O}}\text{H} + \text{M} = \text{H}_2\text{O}_2 + \text{M}$  even though Koert et al. [59] have observed a high sensitivity to this reaction. They found that this reaction is important in controlling the overall reaction rate at the end of the NTC region, and has comparatively little effect at the onset of the NTC region.

Sensitivity analyses were performed by multiplying the rate constants of a particular class of reaction by a factor of two (both forward and reverse rates) and then calculating the percent change in reactivity. In the case of the shock tube experiments of Ciezki and Adomeit [5] for example, we calculated the percent change in ignition delay time compared with the baseline simulation. A positive percent change indicates a longer ignition delay and a decreased overall reaction rate, and a negative change indicates an increased overall reactivity of the system. Three different temperatures were chosen to help indicate sensitivity of each class to the onset, middle and end of the NTC region at an average pressure of 13.5 atm. The reaction rate constants that exhibited the highest sensitivity are shown in Figure 11. Reactions in which we multiplied both forward and reverse rate constants by a factor of two are denoted with an equal to "=" sign between reactants and products and reactions in which we multiplied only the forward rate constant (i.e. effected a change in the equilibrium constant) are denoted with an arrow " $\Rightarrow$ " between reactants and products.

The reaction class with the highest negative sensitivity, and is therefore the most effective in promoting the overall rate of oxidation is reaction type 23, the isomerization of the peroxy-alkylhydroperoxide radical to form a ketohydroperoxide molecule and  $\dot{\text{O}}\text{H}$  radical:



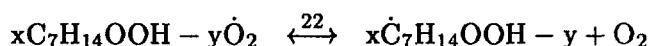
In  $x\text{C}_7\text{H}_{14}\text{OOH} - y\dot{\text{O}}_2$ , x refers to the number of the carbon with the OOH group attached and y refers to the site where the  $\text{O}_2$  group is attached. In  $n\text{C}_7\text{ketxy}$ , x refers to the number of the carbon with the keto group attached and y refers to the site where the hydroperoxy group is attached. We have also observed identical sensitivity to changing the equilibrium constant of this reaction by a factor of two i.e. multiplying the forward rate by two but maintaining the reverse rate at its usual value. This result is expected, as the reverse rate of addition of  $\dot{\text{O}}\text{H}$  radical to the ketohydroperoxide is very slow and is not observed computationally.

Reaction type 23 leads to the formation of reactive  $\dot{\text{O}}\text{H}$  radicals. Subsequent decomposition of the ketohydroperoxide molecule leads to the formation of another  $\dot{\text{O}}\text{H}$  radical and an oxygenated-alkoxy radical, reaction type 24, which is chain branching.



We observe a high negative sensitivity coefficient to this reaction type. At low temperatures the high activation energy barrier (43000 cal/mol) associated with the decomposition of ketohydroperoxide molecules is difficult to overcome and ensures that this reaction occurs very slowly. As fuel oxidation proceeds and the associated heat release raises the reactor temperature, these stable molecules decompose more readily relieving this "bottleneck" and ensuring greater reactivity of the system. This behaviour is, to large degree, responsible for the first stage or "cool-flame" ignition at low temperatures.

We observed a large sensitivity to changing the equilibrium constant of reaction type 22 by a factor of two (i.e. multiplying the reverse addition rate by two but maintaining the forward rate at its usual value).

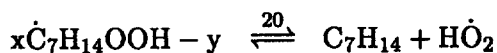


This sensitivity is easily understood, as the addition of hydroperoxy-heptyl radical to  $O_2$  leads preferentially to chain branching and allows fewer hydroperoxy-alkyl radicals to decompose.

The sensitivity coefficients of reaction types 22–24 decrease in importance as the temperature increases because, at higher temperatures, heptyl and hydroperoxy-heptyl radicals decompose more readily *via*  $\beta$ -scission, rather than go through the successive  $O_2$  addition channels which lead to the formation of two reactive  $\dot{O}H$  radicals. These  $\beta$ -scission channels become more accessible because the activation energy barriers associated with these unimolecular reactions are overcome more easily with rising temperature. Also at higher temperatures, the influence of the equilibrium of  $\dot{R} + O_2 \rightleftharpoons R\dot{O}_2$  becomes more important as shown by the sensitivity in Figure 11. The equilibrium shifts from favouring formation of  $R\dot{O}_2$  to reverse reaction,  $\dot{R} + O_2$ . This equilibrium shift further increases the concentration of  $\dot{R}$  which can react *via*  $\beta$ -scission.

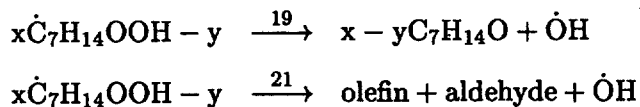
The reaction which is next greatest in promoting the rate of fuel oxidation at low temperatures is H atom abstraction from the fuel by  $\dot{O}H$  radicals. This high negative sensitivity was also observed by Koert et al. in their study on the oxidation of propane. However, as the temperature increases to 950 K and above this reaction type decreases in importance, because a decrease in the rates of reaction classes 22–24 effects a decrease in the production of  $\dot{O}H$  radicals. Thus, a reduced sensitivity to H atom abstraction by  $\dot{O}H$  radicals is observed at higher temperatures.

The production of heptenes and  $H\dot{O}_2$  radicals from hydroperoxy-heptyl radicals, reaction type 20, shows the highest positive sensitivity at 750 K and 950 K:



This reaction has a large inhibiting effect on the overall oxidation rate [59], and plays an important role in producing NTC behaviour as previously described in the literature [70]. This reaction competes with the addition of molecular oxygen to  $\dot{Q}OOH$  described above, consumes one hydroperoxy-heptyl radical and produces the relatively unreactive hydroperoxyl radical and a stable heptene species.

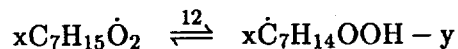
For this same reason, two related reaction types, which are also important in producing NTC behaviour, show a relatively high positive sensitivity coefficient; (1) the production of a cyclic ether and  $\dot{O}H$  radical from  $\dot{Q}OOH$ , reaction type 19, and (2) the  $\beta$ -scission of  $\dot{Q}OOH$  to form an olefin, aldehyde and  $\dot{O}H$  species, reaction type 21.



in  $x-yC_7H_{14}O$ ,  $x$  and  $y$  refer to the position of the C-O bonds in the cyclic ether. The positive sensitivity coefficient for both of these reactions is quite similar but is not as great as that above for the formation of heptene and  $H\dot{O}_2$  species. This is because one relatively reactive  $\dot{O}H$  radical is formed in these reactions which leads to greater overall reactivity than does the formation of the  $H\dot{O}_2$  radical.

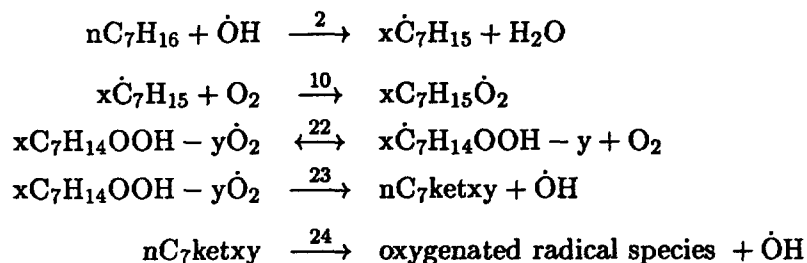
Alkyl radical  $\beta$ -scission, reaction type 3, also shows a positive sensitivity coefficient at 750, 950 and 1100 K. This reaction produces a stable olefin and a relatively unreactive methyl or larger alkyl radical and competes with molecular oxygen addition and the low temperature chain branching reactions, which increase the overall reactivity of the system. This reaction has a high activation energy so that it exhibits higher sensitivities at 950 K and 1150 K than at 750 K. Whether the forward and reverse rate constants are changed by a factor of two or just the forward rate constant, the same sensitivity is obtained. This indicates the calculations are not sensitive to the reverse rate,  $\dot{R}' + \text{olefin}$ .

One very interesting and quite unexpected result of this analysis, was the sensitivity coefficient observed for heptylperoxy radical isomerization, reaction type 12:

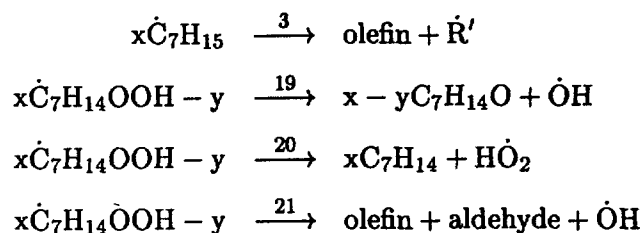


When we multiplied both the forward and reverse rate constants by a factor of two this reaction type showed a *positive* sensitivity coefficient at 750 and 950 K and a small *negative* coefficient at 1100 K. In order to understand why this happens one must consider the products favoured when we increase both of these reaction rate constants. At 750 and 950 K we observe more sensitivity to the reverse isomerization, the formation of heptyl-peroxy radical from hydroperoxy-heptyl radical. Thus, we inhibit the chain branching pathway, which results in lower reactivity and a positive sensitivity coefficient. At 1100 K the reverse is true, we see more sensitivity to the forward isomerization. In this case hydroperoxy-heptyl radicals that are favoured can (1) form an olefin and  $\dot{\text{H}}\text{O}_2$  radical, or (2)  $\beta$ -scission to produce an  $\dot{\text{O}}\text{H}$  radical and an alkoxy radical or (3) form a cyclic ether and  $\dot{\text{O}}\text{H}$  radical. Molecular oxygen addition does not occur as much at 1100 K because this reaction is bimolecular at the activation energy barriers to the  $\dot{\text{Q}}\text{OOH}$  decomposition reactions are easily overcome. These decomposition reactions form  $\dot{\text{O}}\text{H}$  and  $\dot{\text{H}}\text{O}_2$  radicals which are more reactive than  $\dot{\text{C}}\text{H}_3$  or other larger alkyl radicals which may be formed from alkyl radical  $\beta$ -scission, reaction type 3, at 1100 K. Thus reaction type 12 shows a negative sensitivity at 1100 K. This argument is supported by the fact that we observe negative sensitivity coefficients at all three temperatures when only the forward rate constant is multiplied by two i.e. when we change the equilibrium constant as this favours chain branching at 750 and 950 K and leads to more reactive  $\dot{\text{O}}\text{H}$  and  $\dot{\text{H}}\text{O}_2$  radicals at 1100 K.

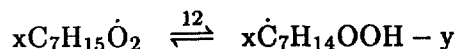
A sensitivity analysis was also performed on the rapid compression machine experiments of Griffiths et al. [9, 10]. In carrying out this analysis we included both the compression and constant volume portions of the experiment but did not include any heat losses to the walls. The results are shown in Figure 12 and report sensitivity at three different ignition delay times. We do not include a consistent compressed gas temperature as the temperature and pressure varied slightly for each sensitivity calculation. The temperatures reached in the baseline simulations were 754.16 K, 790.98 K, and 952.05 K, corresponding to ignition delay times of 3.39 ms, 3.64 ms and 1.99 ms respectively. These sensitivity results are almost identical to those observed in the shock tube of Ciezki and Adomeit [5]. We see high negative sensitivity coefficients at all three 'temperatures' to the reactions that lead to chain branching.



Reactions which inhibit the low temperature chain branching reactions show positive sensitivity coefficients.



It should be noted that again by multiplying both the forward and reverse rate constants of peroxyalkyl radical isomerization, reaction type 12,





by a factor of two we see a positive sensitivity coefficient but when we increase the equilibrium constant to favour the forward isomerization, we see a negative sensitivity coefficient. This is also consistent with the results of Ciezki and Adomeit.

The sensitivity coefficients associated with the RCM experiments of Minetti et al. [12], variable pressure flow reactor experiments of Dryer et al. [20, 22], and the experimental results obtained by Dagaut et al [7, 8] in a JSR are depicted in Figures 13–15 respectively. Foremost, it is clear that the same families of reactions have the same overall influence on the simulations as discussed above for the shock tube results. There is a general trend, especially for Figures 13–15 where the sensitivity seems to be greatest for conditions in the middle of the NTC range. This points out the fact that this is the regime in which the competition between the ketohydroperoxide/chain branching reaction path and the hydroperoxyalkyl decomposition/chain propagation paths is most closely balanced, so a perturbation in this balance has the greatest effect.

## Conclusions

The present study has developed a detailed reaction mechanism for n-heptane oxidation using the best available kinetic data and sound thermochemical analyses. The mechanism has been tested quite thoroughly by comparing computed results with a wide variety of experimental data reported by different authors using a number of experimental techniques. Agreement between computed and measured results was generally very good and suggests strongly that the great majority of the important reaction paths and rate expressions are reasonably correct.

Many of the reaction paths and rate expressions in the mechanism can still be improved considerably. Many of the experimental studies used here for model testing and validation include significantly more data than were used here, and we intend to carry out more thorough analyses in the near future using these data. Further model refinements may be produced through these future efforts.

The model and the accompanying sensitivity analyses have shown the reaction pathways which are particularly important in each regime of pressure, temperature and equivalence ratio. As in previous kinetic modeling by many authors the key to understanding the reaction mechanism is a careful and accurate description of the major chain branching reaction paths and those kinetic processes which compete with the chain branching paths. In the present mechanism, the production and decomposition reactions of ketohydroperoxide molecules were found to provide the important low temperature chain branching, and the hydroperoxyalkyl decomposition reactions provide the major competition.

## Acknowledgement

The authors wish to thank Professor E. Ranzi of Politecnico di Milano for assistance with the lumped model and for support of P. Gaffuri during the period of this work. We would also like to thank Prof. F. Dryer, Dr. R. Minetti, Dr. P. Dagaut and Dr. J. Griffiths for providing us with additional data without which we would not have been able to simulate their experimental results. This work was performed under the auspices of the U.S. Department of Energy by the Lawrence Livermore National Laboratory under contract No. W-7405-ENG-48.

## References

- [1] Vermeer, D. J., Meyer, J. W., and Oppenheim, A. K., *Combust. Flame* 18, 327-336 (1972).
- [2] Coats, C. M., and Williams, A., *Seveteenth Symposium (International) on Combustion*, The Combustion Institute, Pittsburgh, 1978, pp. 611-621.
- [3] Burcat, A.; Farmer, R. F. and Matula, R. A., *Thirteenth Symposium (International) on Shock Tubes and Waves*, (Ch. E. Treanor and J. G. Hall, Eds.), 1981, pp. 826-833.
- [4] Ciezki, H. K., and Adomeit, G., *Sixteenth Symposium (International) on Shock Tubes and Waves*, 1987, pp. 481-486.
- [5] Ciezki, H. K., and Adomeit, G., *Combust. Flame* 93:421-433 (1993).
- [6] Chakir, A., Belliman, M., Boettner J. C., and Cathonnet, M., *Int. J. Chem. Kinet.*, 24:385-410 (1992).
- [7] Dagaut, P., Reuillon, M., and Cathonnet, M., *Combust. Sci. and Tech.* 95:233-260 (1994).
- [8] Dagaut, P., Reuillon, M., and Cathonnet, M., *Combust. Flame* 101:132-140 (1995).
- [9] Griffiths, J. F., Halford-Maw, P. A., and Rose, D. J., *Combust. Flame* 95:291-306 (1993).
- [10] Griffiths, J. F., Hughes, K. J., Schreiber, M., and Poppe, C., *Combust. Flame* 99:533 (1994).
- [11] Cox, A., Griffiths, J. F., Mohamed, C., Curran, H., Pitz, W. J., and Westbrook, C. K. *Twenty-Sixth Symposium (International) on Combustion.*, The Combustion Institute, Pittsburgh, 1996, in press.
- [12] Minetti, R., Carlier, M., Ribaucour, M., Therssen. E., and Sochet, L. R., *Combust. Flame*, 102:298-309 (1995).
- [13] Sahetchian, K. A.; Heiss, A.; Rigny, R. and Ben-Aim, R. I., *J. Chem. Kinet.* 14:1325-1337 (1982).
- [14] Sahetchian, K. A., Blin, N., Rigny, R., Seydi, A., and Murat, M., *Combust. Flame* 79:242-249 (1990).
- [15] Sahetchian, K. A., Rigny, R., and Circan, S., *Combust. Flame* 85:511-514 (1991).
- [16] Leppard, W. R., Society of Automotive Engineers publication SAE-922325, (1992).
- [17] Blin-Simiand, N., Rigny, R., Viossat, V., Circan, S., and Sahetchian, K., *Combust. Sci. and Tech.*, 88:329-348 (1993).
- [18] Cavaliere, A., Ciajolo, A., D'Anna A., Mercogliano, R., and Ragucci, R., *Combust. Flame* 93:279-286 (1993).
- [19] Li, H., Prabhu, S. K., Miller, D. L., and Cernasky, N. P., Society of Automotive Engineers publication SAE-942062, (1994).
- [20] Vermeersch, M. L., Held, T. J., Stein, Y. S., and Dryer, F. L., *SAE Trans.* 100:645 (1991).
- [21] Curran, H. J., Gaffuri, P., Pitz, W. J., Westbrook, C. K., Callahan, C., Dryer, F. L., and Held, T., *Central States/Western States/Mexican Ntl. Sections Comb. Inst.*, 1995, p. 263.
- [22] Callahan, C. V., Held, T. J., Dryer, F. L., Minetti, R., Ribaucour, M., Sochet, L. R., Faravelli, T., Gaffuri, P., and Ranzi, E., *Twenty-Sixth Symposium (International) on Combustion.*, The Combustion Institute, Pittsburgh, 1996, in press.
- [23] Lignola, P. G., Di Maio, F. P., Marzocchiella, A., Mercogliano, R., and Reverchon, E., *Twenty-Second Symposium (International) on Combustion.*, The Combustion Institute, Pittsburgh, 1988, pp. 1625-1633.
- [24] Ciajolo, A., D'Anna, A., and Mercogliano, R., *Combust. Sci. and Tech.* 90:357-371 (1993).
- [25] Chevalier, C., Louessard, P., Müller, U. C., Warnatz, J. *Second Int. Symp. on Diagnostics and Modeling of Combustion in Reciprocating Engines*. The Japanese Society of Mechanical Engineers, Tokyo, 1990, p. 93.
- [26] Chevalier, C., Warnatz, J. and Melenk, H. *Ber. Bunsenges Phys. Chem.* 94:1362 (1990).
- [27] Müller, U. C., Peter, N. and Linan, A. *Twenty-Fourth Symposium (International) on Combustion.*, The Combustion Institute, Pittsburgh, 1992, p. 777.
- [28] Foelsche, R. O., Keen, J. M. and Solomon, W. C. University of Illinois Report No. AAE9307, UIL93-0507.

- [29] Lindstedt, R. P. and Maurice, L. Q. *Combust. Sci. Tech.*, 107:317-353 (1995).
- [30] Bui-Pham, M. and Seshadri, K. *Combust. Sci. Tech.*, 79:293 (1991).
- [31] Ranzi, E., Gaffuri, P., Faravelli, T., and Dagaut, P., *Combust. and Flame*, 103:91-106 (1995).
- [32] Côme, G. M., Warth, V., Glaude, P. A., Fournet, R., Battin-LeClerc, F., and Scacchi, G. *Twenty-Sixth Symposium (International) on Combustion.*, The Combustion Institute, Pittsburgh, 1996, in press.
- [33] Westbrook, C. K., and Dryer, F. L., *Eighteenth Symposium (International) on Combustion.*, The Combustion Institute, Pittsburgh, 1981, pp. 749-767.
- [34] Westbrook, C. K., Warnatz, J., and Pitz, W. J., *Twenty-Second Symposium (International) on Combustion.*, The Combustion Institute, Pittsburgh, 1988, pp. 893-901.
- [35] Westbrook, C. K., Pitz, W. J., and Leppard, W. R., Society of Automotive Engineers publication SAE-912314, (1991).
- [36] Chevalier, C., Pitz, W. J., Warnatz, J., Westbrook, C. K., and Melenk, H., *Twenty-Fourth Symposium (International) on Combustion.*, The Combustion Institute, Pittsburgh, 1992, pp. 92-101.
- [37] Westbrook, C. K., and Pitz, W. J., *Western States Section/ The Combustion Institute*, 1993.
- [38] Ranzi, E., Sogaro, A., Gaffuri, P., Pennati, G., Westbrook, C. K., and Pitz, W. J., *Combust. and Flame*, 99:201-211 (1994).
- [39] Ritter, E. R., and Bozzelli, J. W., *Int. J. Chem. Kinet.*, 23:767-778 (1991).
- [40] Benson, S. W., *Thermochemical Kinetics*. John Wiley and Sons, Inc., New York, 1976.
- [41] Lay, T., Bozzelli, J. W., Dean, A. M., and Ritter, E. R., *J. Phys. Chem.*, 99:14514 (1995).
- [42] Allara, D. L. and Shaw, R., *J. Phys. Chem. Ref. Data*, Vol. 9, No. 3, pp. 523-559 (1980).
- [43] Baulch, D. L., Cobos, C. J., Cox, R. A., Esser, C., Frank, P., Just, TH., Kerr, J. A., Pilling, M. J., Troe, J., Walker, R. W., and Warnatz, J. *J. Phys. Chem. Ref. Data*, 21:411-429 (1992).
- [44] Droege, A. T. and Tully, F. P., *J. Phys. Chem.*, 90:1949 (1986).
- [45] Tully, F. P., Goldsmith, J. E. M., and Droege, A. T., *J. Phys. Chem.*, 90:5932 (1986).
- [46] Westbrook, C. K. and Pitz, W. J., *Combust. Sci. Tech.*, 37:117 (1984).
- [47] Baker, R. R., Baldwin, R. R., and Walker, R. W., *Trans. Faraday Soc.*, 66:2812 (1970).
- [48] Michael, J. V., Keil, D. G., Klemm, R. B., *Int. J. Chem. Kinet.*, 15:705 (1983).
- [49] Edelson, D., and Allara, D. L., *Int. J. Chem. Kinet.*, 12:605 (1980).
- [50] Kerr, J. A., and Parsonage, M. J., *Butterworths*, London (1976).
- [51] Baldwin, R. R., Bennett, J. P., and Walker, R. W. *Sixteenth Symposium (International) on Combustion.*, The Combustion Institute, Pittsburgh, 1977, pp. 1041-1051.
- [52] Walker, R. W. A Critical Survey of Rate Constants for Reactions in Gas-Phase Hydrocarbon Oxidation, in *Reaction Kinetics*, Volume 1 (P. G. Ashmore, editor), The Chemical Society, Burlington House, London, 1975.
- [53] Sundaram, K. M. and Froment, G. F. *Ind. Eng. Chem. Fundam.*, 17:174-182 (1978).
- [54] Walker, R. W. *Twenty-Second Symposium (International) on Combustion.*, The Combustion Institute, Pittsburgh, 1988, pp. 883-892.
- [55] Quelch, G. E., Gallo, M. M., Shen, M., Xie, Y., Schaefer III, H. F., and Moncrieff, D., *J. Am. Chem. Soc.*, 116:4953-4962 (1994).
- [56] Baldwin, R. R., Dean, C. E., and Walker, R. W., *J. Chem. Soc. Faraday Trans. 2*, 82:1445 (1986).
- [57] McAdam, K. G., and Walker, R. W., *J. Chem. Soc. Faraday Trans. 2*, 83:1509 (1987).
- [58] Wagner, A. F., Slagle, I. R., Sarzynski, D., and Gutman, D., *J. Phys. Chem.* 2, 94:1853-1868 (1990).
- [59] Koert, D., Pitz, W. J., Bozzelli J. W., and Cernansky, N. P., *Twenty-Sixth Symposium (International) on Combustion.*, The Combustion Institute, Pittsburgh, 1996, in press.
- [60] Curran, H. J., Gaffuri, P., Pitz, W. J., Westbrook, C. K., and Leppard, W. R., Society of Automotive Engineers publication SAE-952406, (1995).

- [61] Curran, H. J., Pitz, W. J., and Westbrook, C. K., *Twenty-Sixth Symposium (International) on Combustion*, The Combustion Institute, Pittsburgh, 1996, in press.
- [62] Bozzelli, J. W. and Pitz, W. J., *Twenty-Fifth Symposium (International) on Combustion*, The Combustion Institute, Pittsburgh, 1994, pp. 783.
- [63] Bozzelli, J. W., and Ritter, E. R. *Chemical and Physical Processes in Combustion*, The Combustion Institute, Pittsburgh, PA, 1993, 103:459.
- [64] Estimated value based on analogous reactions for similar hydrocarbon fuels.
- [65] Pollard, R. T., *Comprehensive Chemical Kinetics*, (C. H. Bamford and C. F. H. Tipper, Eds), Elsevier, New York, Vol. 17, p. 249, 1977.
- [66] Halstead, M. P., Kirsch, L. J., and Quinn, C. P., *Combust. Sci. Tech.*, 30:45-60 (1977).
- [67] Hu, H., and Keck, J. C., *Society of Automotive Engineers Trans.* 96, (1987).
- [68] Cox, R. A., and Cole, J. A., *Combust. Flame*, 60:109 (1985).
- [69] Griffiths, J. F., *Prog. Energy Combust. Sci.*, 21:25-107 (1995).
- [70] Benson, S. W., *Prog. Energy Combust. Sci.* 7:125-134 (1981).
- [71] Kaiser, E. W., Westbrook, C. K., and Pitz, W. J., *J. Chem. Kinet.*, 18, 655 (1986).
- [72] Baldwin, R. R.; Hisham, M. W. M. and Walker, R. W., *J. Chem. Soc. Farad. Trans. I* 78:1615-1627 (1982).
- [73] Wagner, A. F., Slagle, I. R., Sarzynski, D. and Gutman D., *J. Phys. Chem.* 94:1853-1868 (1990).
- [74] Wallington, T.J., Dagaut, P., Kurylo, M.J., *Chem. Rev.*, 92:667-710 (1992).
- [75] Tsang, W., and Hampson, R. F., *J. Phys. Chem. Ref. Data*, 15:1087 (1987).
- [76] Tsang, W., *J. Phys. Chem. Ref. Data* 20:221-273 (1991).
- [77] Lifshitz, A., and Ben-Hamou, H., *J. Phys. Chem.* 87:1782 (1983).
- [78] Lifshitz, A., and Suslensky, A., *Twenty-Fifth Symposium (International) on Combustion*, The Combustion Institute, Pittsburgh, 1994, pp. 1571-1577.
- [79] Baldwin, R. R., Keen, A., and Walker, R. W., *J. Chem. Soc. Faraday Trans. 1*, 80:435 (1984).
- [80] Dagaut, P., Voisin, D., Cathonnet, M., McGuinness, M., and Simmie, J. M., *Combust. Flame*, 106:62-68 (1996).
- [81] Walker, R. W., *J. Chem. Kinet.* 17:573 (1985).
- [82] Tsang, W., *J. Phys. Chem. Ref. Data* 19:1-68 (1990).
- [83] Tsang, W., *J. Phys. Chem. Ref. Data* 17:887 (1988).
- [84] Gaffuri, P., Curran, H. J., Pitz, W. J., Westbrook, C. K., *Central States/Western States/Mexican Ntl. Sections Comb. Inst.* 233, (1995).
- [85] Marinov, N., and Malte, P. C., *J. Chem. Kinet.* 27:957 (1995).

Radical	Site	Rate expression per H atom			Citation
		$A$	$n$	$E_a$	
$\dot{\text{H}}$	Primary	$9.33 \times 10^6$	2.0	7700.	[46]
$\dot{\text{H}}$	Secondary	$4.55 \times 10^6$	2.0	5000.	[46]
$\dot{\text{H}}$	Tertiary	$1.26 \times 10^{14}$	0.0	7300.	[47]
$\dot{\text{OH}}$	Primary	$1.75 \times 10^9$	0.97	1590.	[44]
$\dot{\text{OH}}$	Secondary	$2.34 \times 10^7$	1.61	-35.	[44]
$\dot{\text{OH}}$	Tertiary	$5.73 \times 10^{10}$	0.51	63.	[45]
$\dot{\text{O}}$	Primary	$7.33 \times 10^5$	2.4	5500.	[48]
$\dot{\text{O}}$	Secondary	$2.35 \times 10^5$	2.5	2230.	[48]
$\dot{\text{O}}$	Tertiary	$1.10 \times 10^{13}$	0.0	3280.	[48]
$\dot{\text{CH}}_3$	Primary	$2.17 \times 10^{11}$	0.0	11600.	[49]
$\dot{\text{CH}}_3$	Secondary	$2.00 \times 10^{11}$	0.0	9500.	[49]
$\dot{\text{CH}}_3$	Tertiary	$1.00 \times 10^{11}$	0.0	7900.	[50]
$\text{HO}\dot{\text{O}}_2$	Primary	$1.34 \times 10^{12}$	0.0	19400.	[51] <sup>a</sup>
$\text{HO}\dot{\text{O}}_2$	Secondary	$1.22 \times 10^{12}$	0.0	17000.	[51] <sup>a</sup>
$\text{HO}\dot{\text{O}}_2$	Tertiary	$2.16 \times 10^{12}$	0.0	14400.	[51] <sup>a</sup>
$\text{CH}_3\dot{\text{O}}$	Primary	$5.27 \times 10^{10}$	0.0	7000.	[52]
$\text{CH}_3\dot{\text{O}}$	Secondary	$5.48 \times 10^{11}$	0.0	5000.	[52]
$\text{CH}_3\dot{\text{O}}$	Tertiary	$1.90 \times 10^{10}$	0.0	2800.	[52]
$\text{O}_2$	Primary	$4.17 \times 10^{12}$	0.0	49000.	[52] <sup>b</sup>
$\text{O}_2$	Secondary	$1.00 \times 10^{13}$	0.0	47600.	[52] <sup>b</sup>
$\text{O}_2$	Tertiary	$2.00 \times 10^{13}$	0.0	41300.	[52] <sup>b</sup>
$\dot{\text{C}}_2\text{H}_5$	Primary	$1.67 \times 10^{10}$	0.0	13400.	[42]
$\dot{\text{C}}_2\text{H}_5$	Secondary	$2.50 \times 10^{10}$	0.0	10400.	[42]
$\dot{\text{C}}_2\text{H}_5$	Tertiary	$1.00 \times 10^{11}$	0.0	7900.	[42]
$\dot{\text{C}}_2\text{H}_3$	Primary	$1.67 \times 10^{11}$	0.0	18000.	[53]
$\dot{\text{C}}_2\text{H}_3$	Secondary	$2.00 \times 10^{11}$	0.0	16800.	[53]
$\dot{\text{C}}_2\text{H}_3$	Tertiary	$2.00 \times 10^{11}$	0.0	14300.	[53]
$\text{CH}_3\dot{\text{O}}_2$	Primary	$2.02 \times 10^{12}$	0.0	20430.	[54] <sup>c</sup>
$\text{CH}_3\dot{\text{O}}_2$	Secondary	$2.02 \times 10^{12}$	0.0	17700.	[54] <sup>c</sup>
$\text{CH}_3\dot{\text{O}}_2$	Tertiary	$2.00 \times 10^{12}$	0.0	14000.	[54] <sup>c</sup>
$\text{R}\dot{\text{O}}_2$	Primary	$2.02 \times 10^{12}$	0.0	20430.	[54] <sup>c</sup>
$\text{R}\dot{\text{O}}_2$	Secondary	$2.00 \times 10^{12}$	0.0	17700.	[54] <sup>c</sup>
$\text{R}\dot{\text{O}}_2$	Tertiary	$2.00 \times 10^{12}$	0.0	16000.	[54] <sup>c</sup>

Table 1: Rate constant expressions for H atom abstraction from the fuel.  $\text{cm}^3\text{-mol-sec-cal}$  units

a:  $A$ -factors adjusted from original values of  $1.0 \times 10^{12}$ .

b: As recommended by [52],  $E_a \approx \Delta H$ . Overall  $A$ -factor of  $4.0 \times 10^{13}$  [52] was partitioned between  $1^\circ$ ,  $2^\circ$ , and  $3^\circ$ .

c: Analogy with  $\text{RH} + \text{HO}_2$ .  $A$ -factor has been adjusted down from  $1.8 \times 10^{12}$ .

Isomerization	Ring Size	Rate expression		
		$\mathcal{A}$	$n$	$\mathcal{E}_a$
$1C_7H_{15} \rightleftharpoons 2C_7H_{15}$	3	$5.48 \times 10^8$	1.62	38760.
reverse		$1.74 \times 10^7$	2.01	41280.
$1C_7H_{15} \rightleftharpoons 3C_7H_{15}$	4	$1.39 \times 10^9$	0.98	33760.
reverse		$4.41 \times 10^7$	1.38	36280.
$1C_7H_{15} \rightleftharpoons 3C_7H_{15}$	6	$4.28 \times 10^{11}$	-1.05	11760.
reverse		$1.36 \times 10^{10}$	-0.66	14280.
$1C_7H_{15} \rightleftharpoons 4C_7H_{15}$	5	$2.54 \times 10^9$	0.35	19760.
reverse		$1.61 \times 10^8$	0.74	22280.
$2C_7H_{15} \rightleftharpoons 3C_7H_{15}$	3	$9.59 \times 10^8$	1.39	39700.
reverse		$9.59 \times 10^8$	1.39	39700.
$2C_7H_{15} \rightleftharpoons 3C_7H_{15}$	5	$3.22 \times 10^9$	0.13	20700.
reverse		$3.22 \times 10^9$	0.13	20700.
$2C_7H_{15} \rightleftharpoons 4C_7H_{15}$	4	$1.76 \times 10^9$	0.76	34700.
reverse		$3.50 \times 10^9$	0.76	34700.
$3C_7H_{15} \rightleftharpoons 4C_7H_{15}$	3	$6.04 \times 10^8$	1.39	39700.
reverse		$1.20 \times 10^9$	1.39	39700.

Table 2: Rate constant expressions for  $C_7$  alkyl radical isomerization reactions.  $\text{cm}^3\text{-mol-sec-cal}$  units

Reaction	Rate expression			Citation
	$\mathcal{A}$	$n$	$\mathcal{E}_a$	
$\text{Olefin} + \dot{\text{H}} = \text{Alkenyl} + \text{H}_2$	$1.00 \times 10^{12}$	0.00	3900.	[64]
$\text{Olefin} + \dot{\text{O}}\text{H} = \text{Alkenyl} + \text{H}_2\text{O}$	$1.00 \times 10^{12}$	0.00	1230.	[64]
$\text{Olefin} + \dot{\text{O}} = \text{Alkenyl} + \dot{\text{O}}\text{H}$	$1.00 \times 10^{12}$	0.00	4000.	[64]
$\text{Olefin} + \dot{\text{C}}\text{H}_3 = \text{Alkenyl} + \text{CH}_4$	$2.00 \times 10^{11}$	0.00	7300.	[64]

Table 3: Rate constant expressions for H atom abstraction from  $C_7$  olefin.  $\text{cm}^3\text{-mol-sec-cal}$  units

Reaction	Rate expression			Citation
	$\mathcal{A}$	$n$	$\mathcal{E}_a$	
$\text{Olefin} + \dot{\text{O}} = \text{products}$	$2.00 \times 10^{10}$	0.00	1050.	[64]
$\text{Olefin} + \dot{\text{O}}\text{H} = \text{products}$	$2.00 \times 10^{10}$	0.00	4000.	[64]

Table 4: Rate constant expressions for  $\dot{\text{O}}\text{H}$  and  $\dot{\text{O}}$  radical addition to  $C_7$  olefin.  $\text{cm}^3\text{-mol-sec-cal}$  units

Number of ring members	Ring strain (kcal mol <sup>-1</sup> )
5	8.6
6	2.8
7	0.0
8	2.8

Table 5: Number of atoms in T. S. ring structure versus ring strain energy

Ring size	Site	Rate expression (per H atom)		
		$\mathcal{A}$	$n$	$\mathcal{E}_a$
5	Primary	$2.98 \times 10^{12}$	0.0	29700.
	Secondary	$2.98 \times 10^{12}$	0.0	27900.
	tertiary	$2.59 \times 10^{12}$	0.0	25400.
6	Primary	$2.47 \times 10^{11}$	0.0	23900.
	Secondary	$2.48 \times 10^{11}$	0.0	22150.
	tertiary	$2.16 \times 10^{11}$	0.0	19700.
7	Primary	$2.06 \times 10^{10}$	0.0	21100.
	Secondary	$2.06 \times 10^{10}$	0.0	19350.
	tertiary	$1.80 \times 10^{10}$	0.0	16400.
8	Primary	$1.72 \times 10^9$	0.0	23900.
	Secondary	$1.72 \times 10^9$	0.0	22150.
	tertiary	$1.50 \times 10^9$	0.0	19700.

Table 6: Rate constant expressions for  $\text{RO}_2$  isomerization reactions. cm<sup>3</sup>-mol-sec-cal units

Epoxide Ring size	Rate expression		
	$\mathcal{A}$	$n$	$\mathcal{E}_a$
3	$3.00 \times 10^{11}$	0.0	22000.
4	$2.50 \times 10^{10}$	0.0	15250.
5	$2.08 \times 10^9$	0.0	6500.
6	$1.50 \times 10^8$	0.0	1800.

Table 7: Rate constant expressions for cyclic ether formation from  $\dot{\text{Q}}\text{OOH}$  radicals. cm<sup>3</sup>-mol-sec-cal units

Ring size	Site	Rate expression (per H atom)		
		$\mathcal{A}$	$n$	$\mathcal{E}_a$
5	Primary	$1.49 \times 10^{12}$	0.0	26700.
	Secondary	$1.49 \times 10^{12}$	0.0	24900.
6	Primary	$1.24 \times 10^{11}$	0.0	20900.
	Secondary	$1.24 \times 10^{11}$	0.0	19150.
7	Primary	$1.03 \times 10^{10}$	0.0	18100.
	Secondary	$1.03 \times 10^{10}$	0.0	16350.
8	Primary	$8.60 \times 10^8$	0.0	20900.
	Secondary	$8.60 \times 10^8$	0.0	19150.

Table 8: Rate constant expressions for  $\dot{\text{O}}_2\text{QOOH}$  isomerization reactions.  $\text{cm}^3\text{-mol-sec-cal}$  units

Radical	Site	Rate expression (per H atom)		
		$\mathcal{A}$	$n$	$\mathcal{E}_a$
H-C-C $\dot{\text{O}}\text{H}$	Primary	$3.83 \times 10^7$	1.53	775.
	Secondary	$2.34 \times 10^7$	1.61	-35.
	Tertiary	$5.73 \times 10^{10}$	0.51	64.
$\text{H}\dot{\text{O}}_2$	Primary	$3.33 \times 10^3$	2.55	15500.
	Secondary	$7.40 \times 10^3$	2.60	13910.
	Tertiary	$3.61 \times 10^3$	2.55	10532.
H-C-O $\dot{\text{O}}\text{H}$	Primary	$9.50 \times 10^7$	1.61	-35.
	Secondary	$8.84 \times 10^9$	1.00	-149.
	Primary	$3.00 \times 10^4$	2.60	13910.
$\text{H}\dot{\text{O}}_2$	Secondary	$1.08 \times 10^4$	2.55	10532.

Table 9: Rate constant expressions for H atom abstraction from cyclic ether by  $\dot{\text{O}}\text{H}$  and  $\text{H}\dot{\text{O}}_2$ .  $\text{cm}^3\text{-mol-sec-cal}$  units



## Figure Captions

**Figure 1:** (1,5) H atom isomerization *via* transition state ring structure.

**Figure 2:** (1,6) H atom isomerization forming ketohydroperoxide +  $\dot{\text{O}}\text{H}$ .

**Figure 3:** Lumped kinetic scheme of the primary oxidation reactions.

**Figure 4:** 0.14% n-heptane oxidation at 12.5 atm,  $\phi = 1.0$ ,  $\tau = 1.8$  s in a PFR. Experimental results (points) [20, 22] vs model predictions for (a) oxygenates and (b) heat release. Dashed line corresponds to open circles.

**Figure 5:** 0.1% n-heptane oxidation at 10 atm,  $\phi = 1.0$ ,  $\tau = 1$  s in a JSR. Experimental (points) [7, 8] and model predicted mole fraction for some oxygenated compounds, n-heptenes and furans. Dashed line corresponds to open circles.

**Figure 6:** 0.1% n-heptane oxidation at  $\tau = 1$  s in a JSR. Experimental (points) [7, 8] and model predicted conversion with influence of (a) equivalence ratio and (b) pressure. Dashed line corresponds to open circles.

**Figure 7:** Experimental (points) (a) [1], (b) [2] and model predicted ignition delay times. Dashed line corresponds to open circles.

**Figure 8:** 1.79% n-heptane oxidation behind reflected shock waves in 80%  $\text{N}_2$ . Comparison between experimental (points) [5] and model prediction.  $\tau$  is the ignition delay time. Dashed line corresponds to open circles.

**Figure 9:** (a) Model predicted temperatures profiles in rapid compression machine experiments [12] depicting NTC behaviour. (b) Experimental (points) [12] and model prediction (lines) ignition delay time ( $\bullet$ ) and first ignition ( $\circ$ ). Time zero is the time at the end of compression and  $T_c$  is the temperature at the end of compression. Dashed line corresponds to open circles.

**Figure 10:** (a) Experimental (points) [9, 10] and model predicted ignition delay times. The terms 'reactive' and 'unreactive' refer only to modeling of the compression stroke portion of each simulation. (b) Pressure histories for unreactive case with n-heptane :  $\text{N}_2$  : Ar = 1 : 20 : 32.5. Open circles refer to experiments and the solid line to the calculation using the heat transfer coefficient selected, see text.

**Figure 11:** Sensitivity coefficients in a shock tube [5]. Stoichiometric fuel in air,  $P_5 = 13.5$  bar.

**Figure 12:** Sensitivity coefficients in a RCM [9, 10]. Stoichiometric fuel in diluent 'air'.  $T_i = 340$  K,  $P_i = 250$  torr, CR = 11:1.

**Figure 13:** Sensitivity coefficients in a RCM [12]. Stoichiometric fuel in diluent 'air'.  $T_i = 355$  K,  $P_i = 162$  torr, CR = 9.8:1.

**Figure 14:** Sensitivity coefficients in a flow reactor [21, 22]. 0.14% n-heptane oxidation at 12.5 atm,  $\phi = 1.0$ ,  $\tau = 1.8$  s.

**Figure 15:** Sensitivity coefficients in a JSR [7, 8]. 0.1% n-heptane oxidation at 10 atm,  $\phi = 1.0$ ,  $\tau = 1$  s.

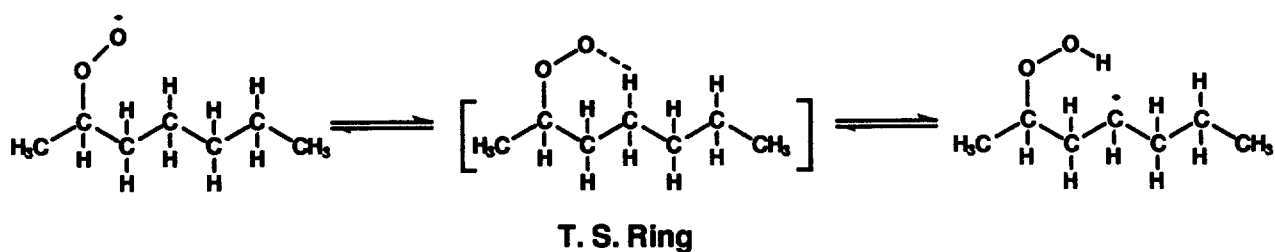


Figure 1: (1,5) H atom isomerization *via* transition state ring structure

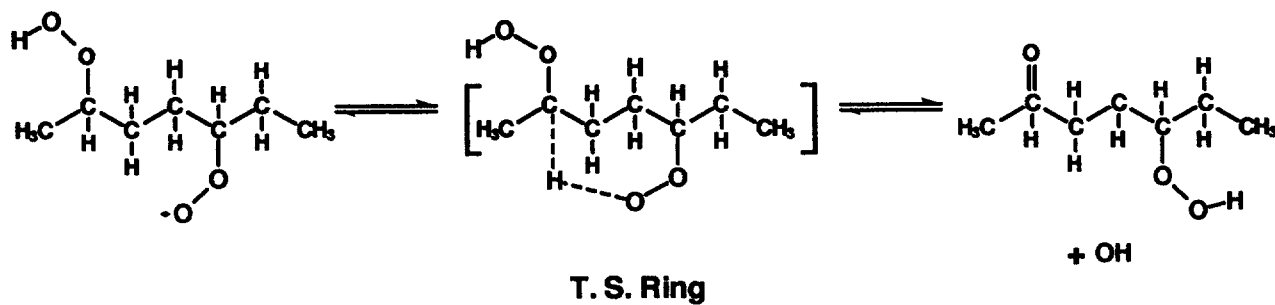


Figure 2: (1,6) H atom isomerization forming ketohydroperoxide +  $\dot{\text{O}}\text{H}$

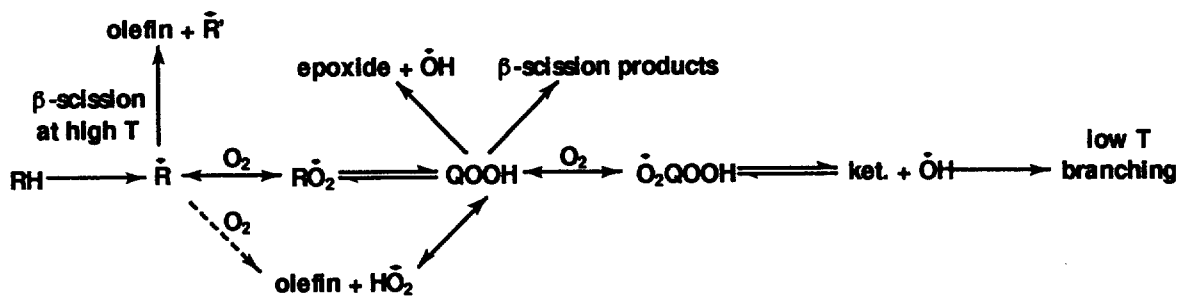


Figure 3: Lumped kinetic scheme of the primary oxidation reactions

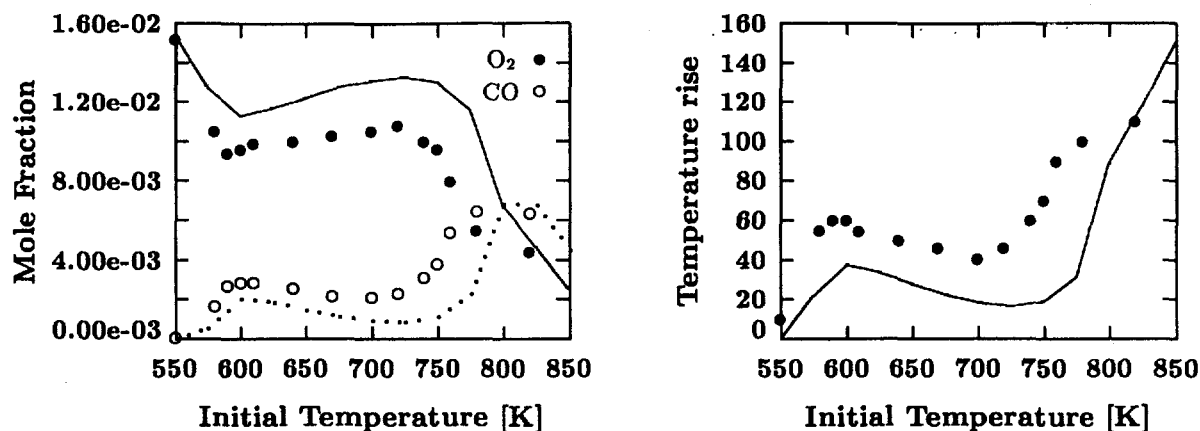


Figure 4: 0.14% n-heptane oxidation at 12.5 atm,  $\phi = 1.0$ ,  $\tau = 1.8$  s in a PFR. Experimental results (points) [20, 22] vs model predictions for (a) oxygenates and (b) heat release. Dashed line corresponds to open circles.

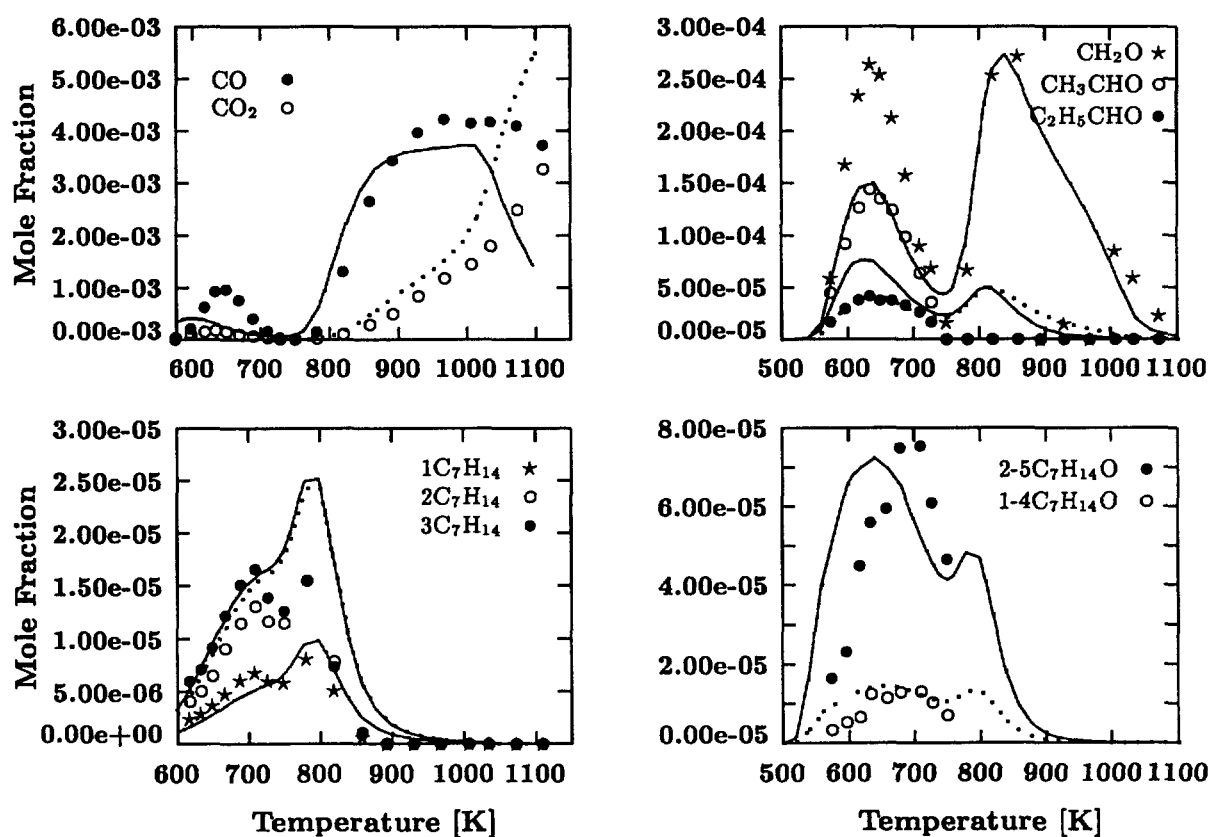


Figure 5: 0.1% n-heptane oxidation at 10 atm,  $\phi = 1.0$ ,  $\tau = 1$  s in a JSR. Experimental (points) [7, 8] and model predicted mole fraction for some oxygenated compounds, n-heptenes and furans. Dashed line corresponds to open circles.

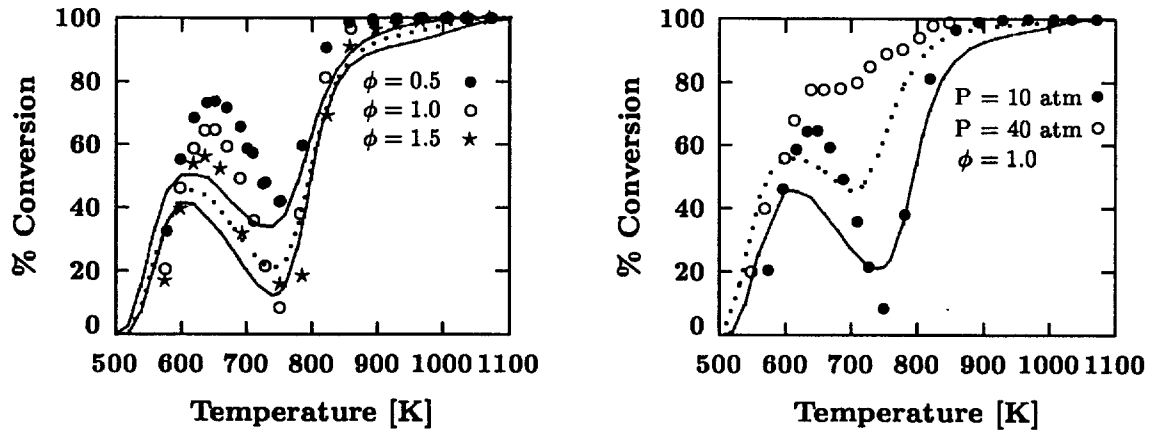


Figure 6: 0.1% n-heptane oxidation at  $\tau = 1$  s in a JSR. Comparison between experimental (point) [7, 8] and model predicted conversion with influence of (a) equivalence ratio and (b) pressure. Dashed line corresponds to open circles.

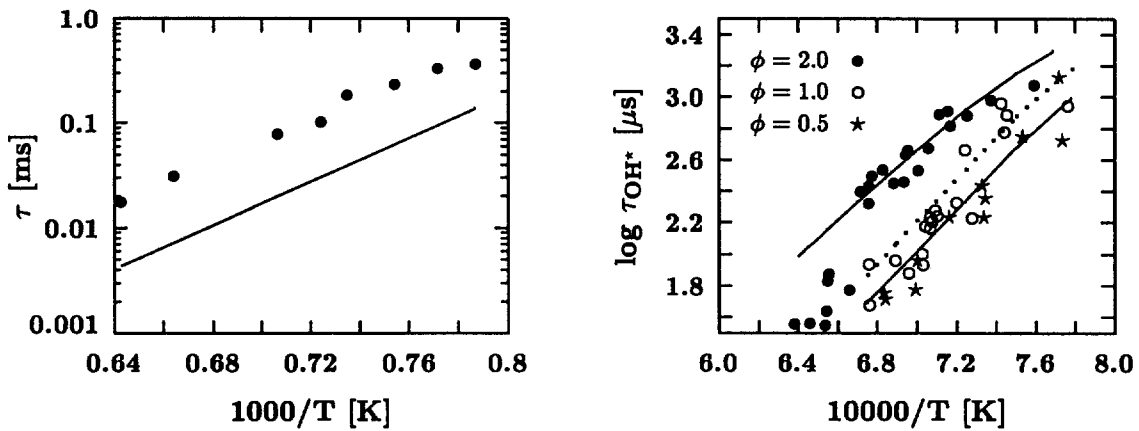


Figure 7: Experimental (points) (a) [1], (b) [2] and model predicted ignition delay times. Dashed line corresponds to open circles.

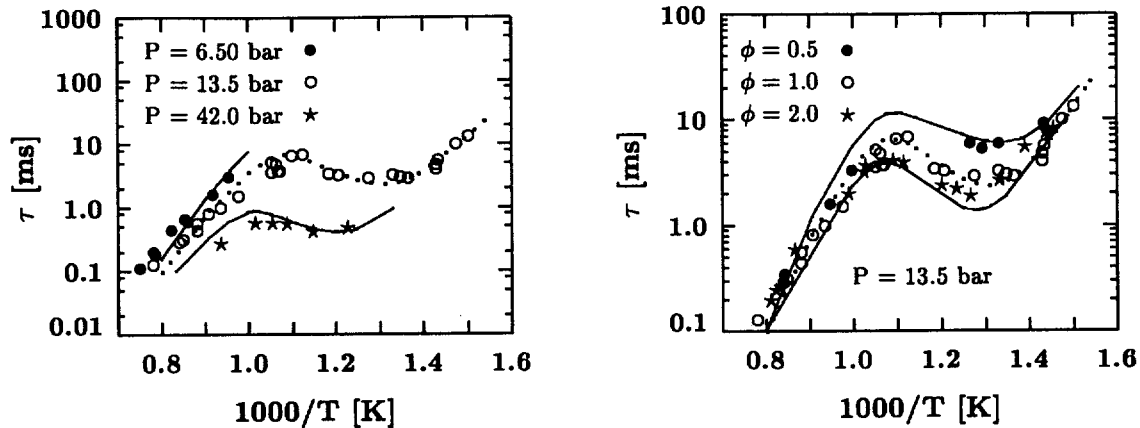


Figure 8: 1.79% n-heptane oxidation behind reflected shock waves in 80% N<sub>2</sub>. Comparison between experimental (points) [5] and model prediction.  $\tau$  is the ignition delay time. Dashed line corresponds to open circles.

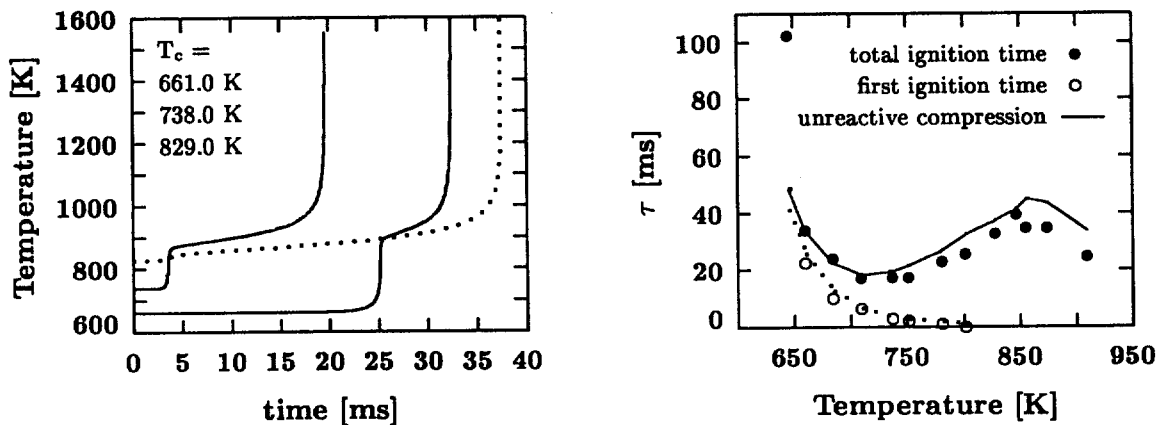


Figure 9: (a) Model predicted temperatures profiles in rapid compression machine experiments [12] depicting the NTC behaviour. (b) Experimental (points) [12] and model prediction (lines) ignition delay time ( $\bullet$ ) and first ignition ( $\circ$ ). Time zero is the time at the end of compression and  $T_c$  is the temperature at the end of compression. Dashed line corresponds to open circles.

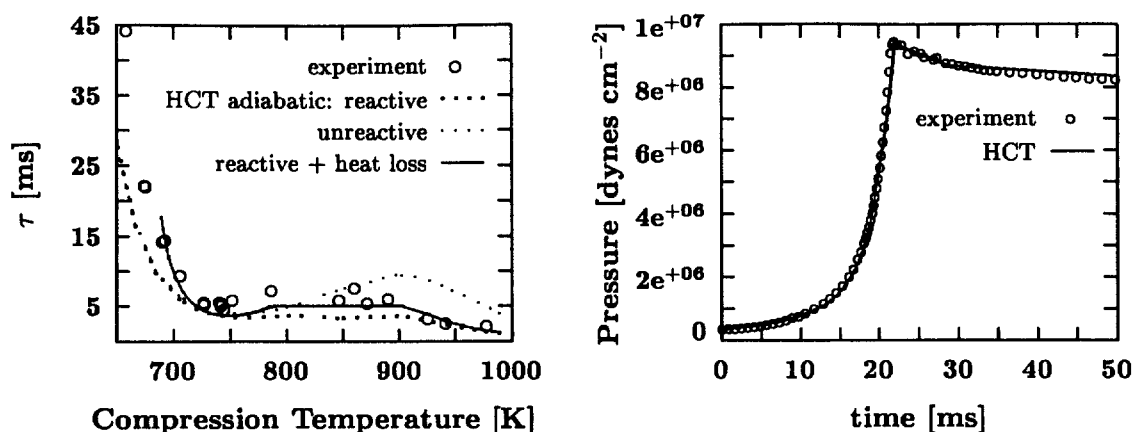


Figure 10: (a) Experimental (points) [9, 10] and model predicted ignition delay times. The terms 'reactive' and 'unreactive' refer only to the simulation of the compression stroke portion of each simulation. (b) Pressure histories for unreactive case with n-heptane : N<sub>2</sub> : Ar = 1 : 20 : 32.5. Open circles refer to experiments and the solid line to the calculation using the heat transfer coefficient selected, see text.

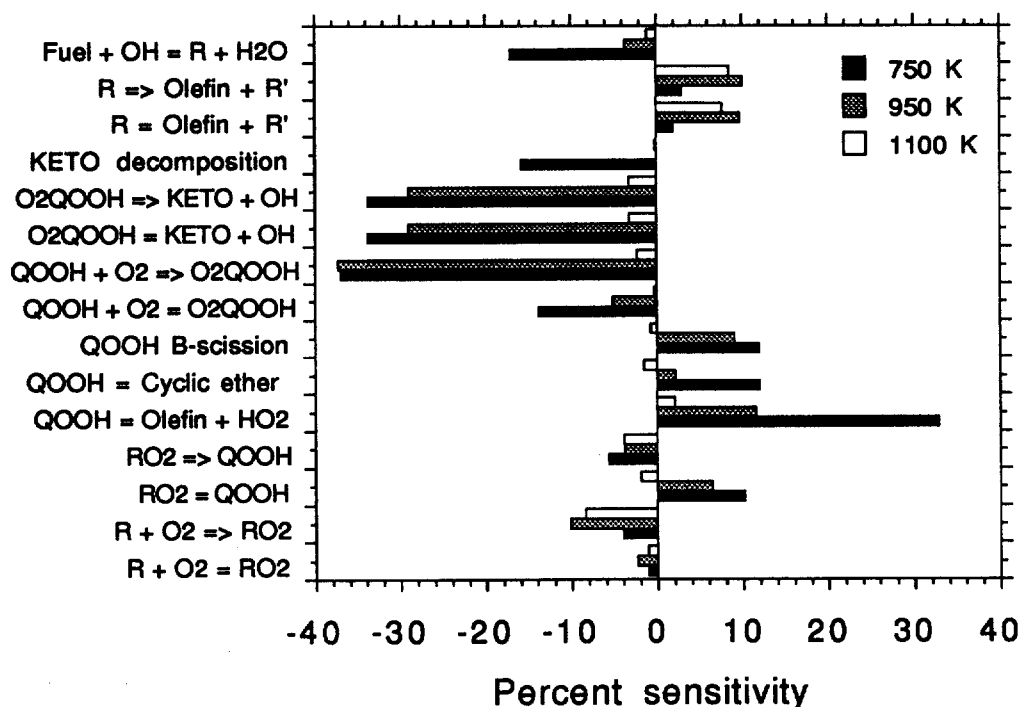


Figure 11: Sensitivity coefficients in a shock tube [5]. Stoichiometric fuel in air,  $P_5 = 13.5$  bar.

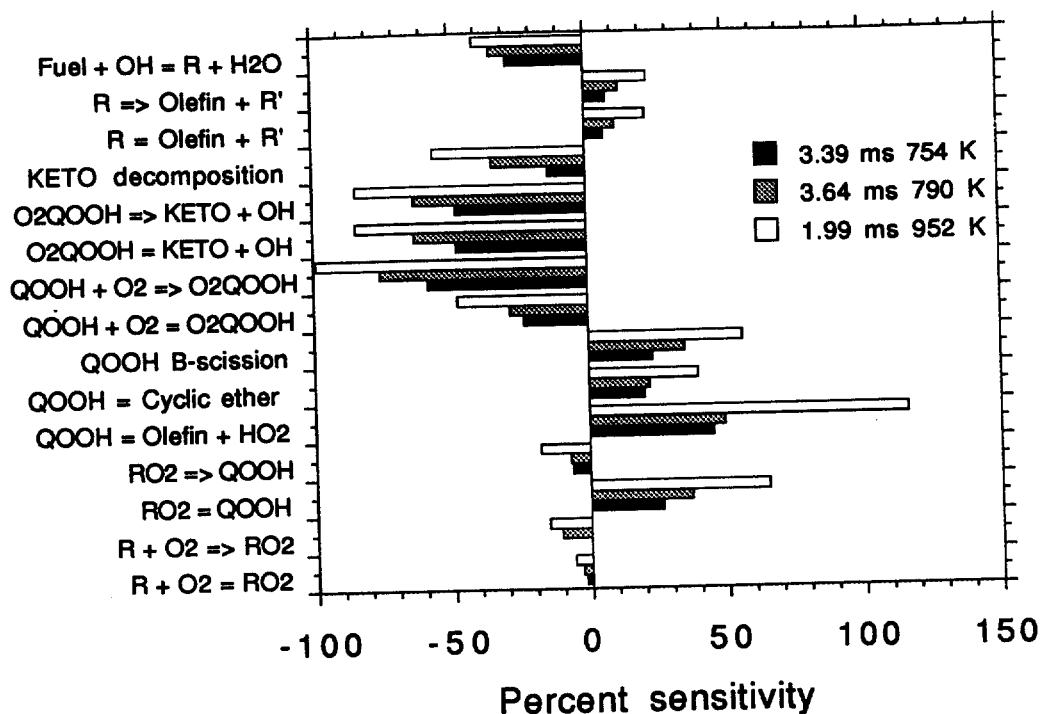


Figure 12: Sensitivity coefficients in a RCM [9, 10]. Stoichiometric fuel in diluent 'air'.  $T_i = 340$  K,  $P_i = 250$  torr, CR = 11:1.

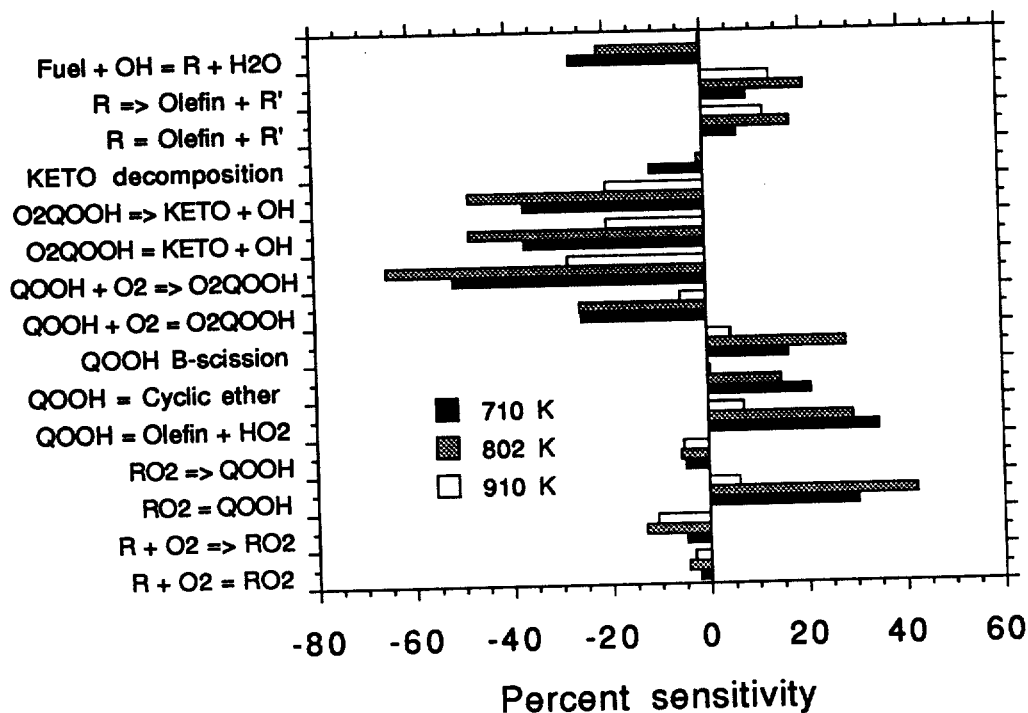


Figure 13: Sensitivity coefficients in a RCM [12]. Stoichiometric fuel in diluent 'air'.  $T_i = 355$  K,  $P_i = 162$  torr, CR = 9.8:1.

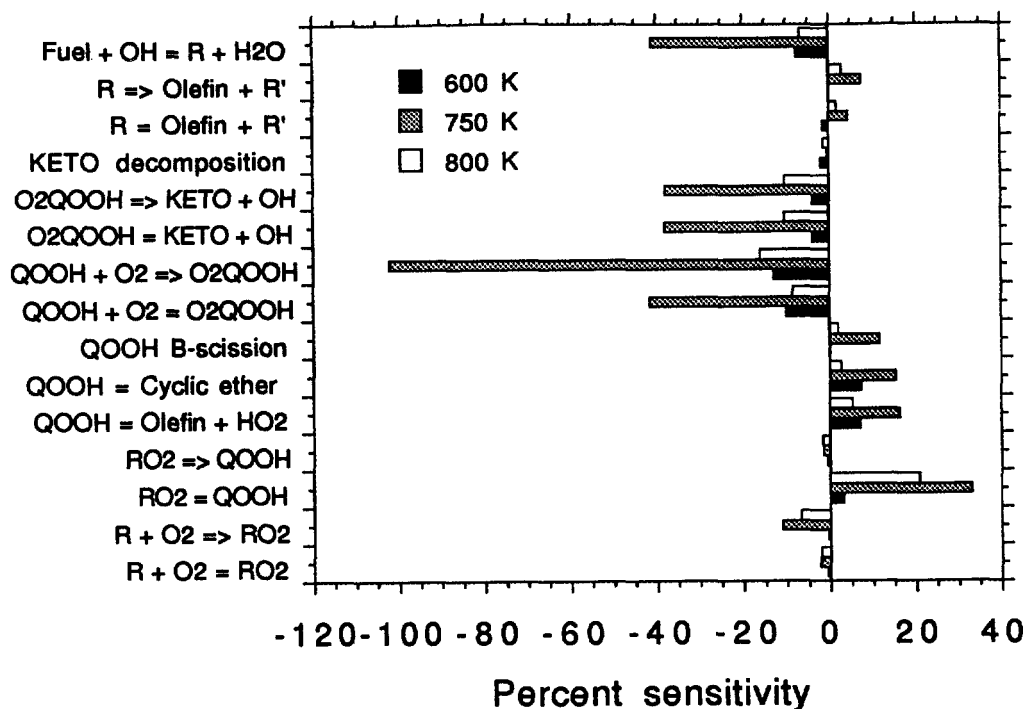


Figure 14: Sensitivity coefficients in a flow reactor [21, 22]. 0.14% n-heptane oxidation at 12.5 atm,  $\phi = 1.0$ ,  $\tau = 1.8$  s.

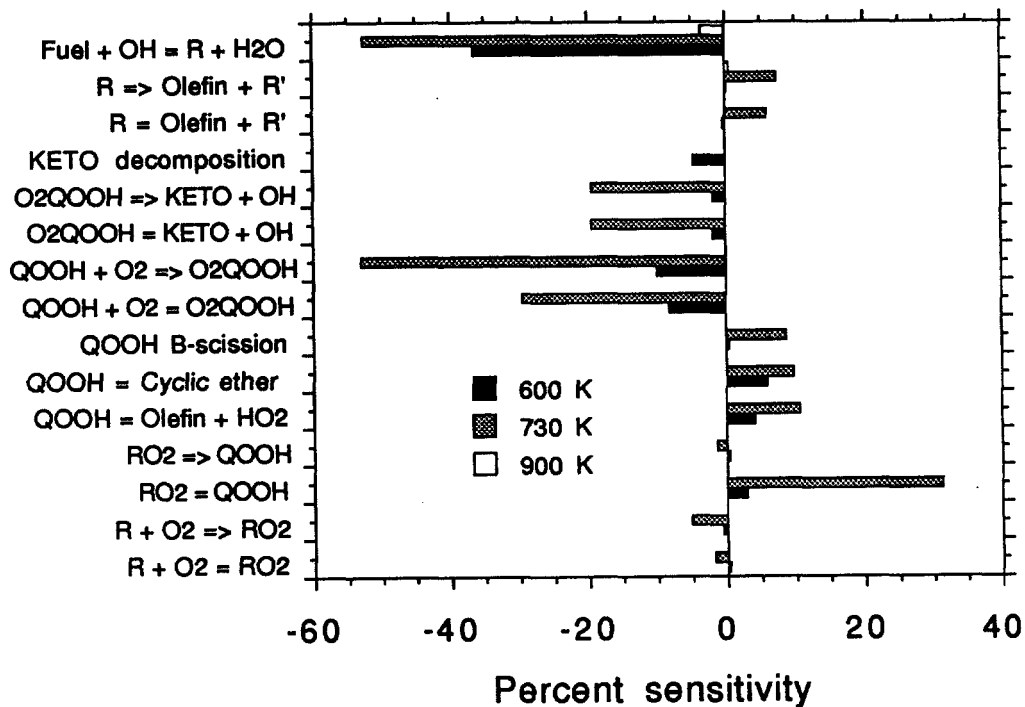


Figure 15: Sensitivity coefficients in a JSR [7, 8]. 0.1% n-heptane oxidation at 10 atm,  $\phi = 1.0$ ,  $\tau = 1$  s.